國 立 交 通 大 學

電信工程學系

碩士論文

新式的多模諧振腔濾波器

Novel Multiple-mode Resonator Filters

研究生：林逸亭

指導教授：張志揚　博士

中華民國　九十七　年　六　月

新式的多模諧振腔濾波器

Novel Multiple-mode Resonator Filters

研 究 生：林逸亭　　　　　Student：Yi-Ting Lin

指導教授：張志揚 博士　　　Advisor：Dr. Chi-Yang Chang

國立交通大學

電信工程學系

碩士論文

A Thesis
Submitted to Department of Communication Engineering
College of Electrical and Computer Engineering
National Chiao Tung University
In Partial Fulfillment of the Requirements
for the Degree of
Master of Science
In
Communication Engineering
June 2008
Hsinchu, Taiwan, Republic of China

中華民國 九十七 年 六 月

新式的多模諧振腔濾波器

研究生：林逸亭　　　　　　　　指導教授：張志揚 博士

國立交通大學電信工程學系

摘要

　　本篇論文提出一種新式的多模態諧振腔濾波器，其主要的特點是具有一個可調整的傳輸零點和大範圍的上止帶，設計方法是將濾波器的諧振頻率調到與 Chebyshev 通帶的傳輸極點相同位置，當我們將耦合量增強，便可產生一個形似 Chebyshev 的頻率響應，可調的傳輸零點由傳輸零點頻率的四分之一波長開路支線傳輸線產生，且此開路支線傳輸線並聯一個電抗，即決定傳輸零點出現在下止帶或上止帶，本篇中有三個 2.45GHz 三模態諧振腔濾波器的設計，量測結果皆與模擬相符合。

　　本篇有另一個濾波器設計方法是使用中間為並聯電抗或串連電納，兩邊為阻抗不相等傳輸線，所形成的 K 倒反器或 J 倒反器來合成濾波器，傳統的方法是使兩邊的傳輸線阻抗相等，因此，我們的設計更為靈活。我們將重點放在 K 倒反器上，J 倒反器可同理推得，跟上一個主題相仿，此處也有一個由傳輸零點頻率的 $\lambda/4$ 開路支線傳輸線所產生的可調傳輸零點，此傳輸線可視為並聯電抗，在兩端加上兩段不同度數、不同阻抗的傳輸線，等效成一個 K 倒反器，本篇中實作兩個 2.45GHz 的三階濾波器以驗證理論。
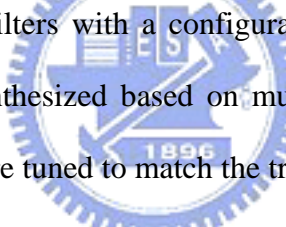
Novel Multiple-mode Resonator Filters

Student: Yi-ting Lin   Advisor: Dr. Chi-Yang Chang

Department of Communication Engineering
National Chiao-Tung University

Abstract

Novel planar bandpass filters with a configurable finite transmission zero and wide upper stop-band are synthesized based on multimode resonator property. The resonances of the resonators are tuned to match the transmission poles of a Chebyshev pass-band in order to create Chebyshev-like response while enhancing the coupling. The transmission zero at finite frequency is brought about by a open-circuit stub with quarter-wavelength of zero frequency. Additionally, the open-circuit stub connecting a shunt reactance can be used to allocate that the transmission zero in the lower or the upper stopband. Tri-mode bandpass filters with the transmission zero on the different sides of the passband are designed. The measured results both show good agreement with simulated responses.

Another design included in this article is the filter with K or J inverter making use of unequal impedance microstip lines with shunt reactance or series susceptance in between. It's more flexible and much different from the conventional design having equal impedance microstrip lines on the both sides. We discuss the K inverter design

only since the design guidelines are the same as those of the J inverter. A centered open-circuit stub is taken to be the reactance and utilized to tune transmission zero position. Third-order band-pass filters with transmission zeros on the different sides of the passband are designed and measured to validate the approach.

誌謝

首先必須感謝指導教授張志揚博士，在兩年的碩士生涯中，給予適時的教導與指引，幫助我們完成論文，平時也跟我們一同用餐、爬山，有如朋友一般，能有這樣的良師益友，真是我的一大福氣。

當然也要感謝學長跟同學們，小谷、雄哥、哲慶、建育、梁八幾位實驗室的學長，在研究上給予許多的提點，錞哥、銘哥、威綸、智皓、憲文這些同窗們，互相勉勵在實驗室度過了兩年，巴里、雅惠、郁文、阿冷讓我當了很久女二 484 的偽室友，還有菁偉、澎澎、小花、useful 等 912 的朋友們，一起吃吃喝喝到處玩，絕對不能漏掉的是小胖，不但容忍我的任性和壞脾氣，要當我的車伕，還教我排版軟體怎麼用，我才可以把論文很漂亮的呈現出來。

最後要謝謝我的家人，親愛的爸爸永遠都給予最大的鼓勵和支持，常常幫我準備一些補品，，媽媽和外婆在天堂裡，一定也有為我禱告，最希望看我拿到碩士的奶奶雖然在口試前幾週不幸過世，但我相信她在天上也能感受到這份喜悅，還有三位姐姐葳亭、憶君、珍瑜的疼愛，也讓我溫暖在心頭，只能說是大家滿滿的愛，讓我順利的完成碩士論文。

Contents

List of Figures

vi

Chapter 1

Introduction

1.1 Motivation

My interest in multimode resonator filter comes from some of its attractive features such as compact planar structure, high selectivity, and simple design guidelines, which are essential for applications in rapidly growing wireless communications. Hence, papers relative to the subject have been studied in this thesis. The foundation of multimode resonator filter designing rules has been established by the predecessors, that is, we could follow the way they paved for us. However, we need to indicate our originality by advancing a brand-new idea.

1.2 Introduction to Multimode Resonator Filter

MMR filter is abbreviated from Multiple-mode Resonator Filter. Recently, a lot of researches involved MMR filters have been published. Its main concept is gathering several resonant modes of the resonator to form the pass-band. As a result, we first need to find an appropriate circuit that can contribute two or more resonances at different frequencies. Plurality of the presented paper chose the stepped-impedance resonator (SIR) as

1

the bulk of the filter due to its versatile resonant characteristics. Its resonant frequencies can be easily altered by tuning its geometric parameters. However, instead of stepped-impedance resonator,we provide a novel resoantor structure to implement multimode resonator filters. For further details, one can refer to Chapter 2.

1.3 Introduction to J and K inverter

As we all know that it is often desirable to have all series or all shunt elements in filter implementation. We can use impedance (K) inverters or admittance (J) inverters to do the job. J and K inverters are useful for band-pass or band-stop filters especially with narrow bandwidths($<10\%$). Fig. 1-1 and 1-2 are the basic operation of impedance and admittance inverters. Concerning about the K inverter in the graph, if the load has positive reactance (inductors), it will seem to have negative reactance (capacitors) at the output by inserting the K inverter. There are many types of network to realize J and K inverters. One of the commonly used network is a shunt impedance for a K-inverter or a series admittance for a J-inverter where two equal characteristic impedance transmission line resonators locate on each side of the inverter. The design formulas are well developed[12] for these inverters. Here, we developed design formulas for two resonators with different characteristic impedances. Our discussion briefly starts from the here and will be completed in the Chapter 3.
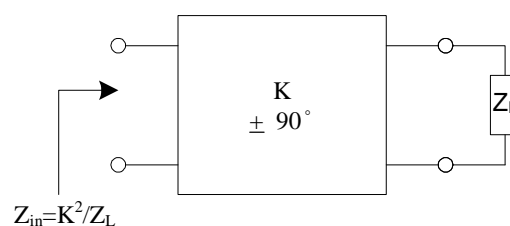
Figure 1-1: Basic operation of K inverter

$Y_{in} = J^2/Y_L$
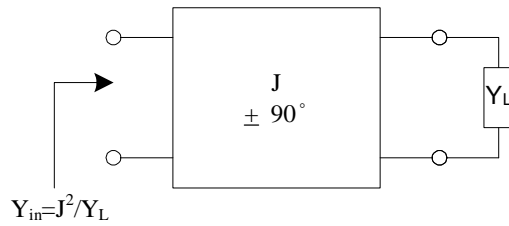
Figure 1-2: Basic operation of J inverter

1.4 Introduction to Wireless LAN

A wireless LAN or WLAN is short for wireless local area network, which links two or more computers without using wires. This gives users the ability to move around within a broad coverage area and still be connected to the network.

For the home user, wireless has become popular due to ease of installation, and location freedom with the gaining popularity of laptops. Many coffee shops or malls have begun to offer wireless access to allure their customers. Thus, large wireless network business is being put up in many cities.

The majority of computers sold to consumers today come pre-equipped with all necessary wireless LAN technology because of their convenience, cost efficiency, and ease of integration with other networks. However, wireless LANs may have some limitations about security, range, reliability, and speed for a given networking situation.

The IEEE standard that regulates WLAN technology is IEEE 802.11 which has gone through several generations since 1997. Some protocol of 802.11 that their products have been available in the market are summarized as follows,

3

Protocol	Release Date	Operation Frequency	Indoor Radius Range	Outdoor Radius Range
802.11a	October 1999	5 GHz	~35 meters	~120 meters
802.11b	October 1999	2.4-2.5 GHz	~38 meters	~140 meters
802.11g	June 2003	2.4-2.5 GHz	~38 meters	~140 meters
802.11n	June 2009 (est.)	2.4 GHz,5 GHz	~70 meters	~250 meters

Figure 1-3: Protocals of 802.11

Evidently, the 2.4 GHz ISM band is very popular for use. In consequence, most of our experiment have made in 2.4 GHz band foreseeing their future applications.

Chapter 2

Multimode Resonator Filters

2.1 Previous Works of Multimode Resonator Filters

The method of design filters using multimode cavity initially appeared in [2] that the first two resonant modes of the MMR together with enhanced I/O parallel-coupled lines will construct wide pass-band with four transmission poles. In [3], the first three resonant modes of an MMR has been newly utilized to construct the pass-band with five transmission poles. Basically following the work in [2] and [3], MMRs in [4]-[6] were properly modified in configuration in order to match its first three resonant modes to the lower-end, center, and upper-end of the desired pass-band. When coupling degree of the input/output parallel coupled lines is boosted, good pass-band performance are realized. Setting up the coupling peak of quarter-wavelength parallel coupled lines at the center frequency, the three types of planar band-pass filters were implemented on the traditional microstrip line[4],on aperture-backed microstrip line[5], and on hybrid microstrip/CPW[6]. Five pole filters can be synthesized with a single triple-mode SIR and an excitation structure with strong coupling. The impedance junctions between SIR and the excitation structure may create two more transmission poles.

However, the researches mentioned before didn't have a systematical design procedure. Not until the MMR reported in [7] was proposed could we follow the clear design guideline. The paper developed a systematical procedure for synthesizing broadband band-pass filters using single or plural multiple-mode SIRs. For plural multiple-mode SIRs design, each SIRs is viewed as a multiple-mode resonator which contribute two or three resonant modes to the circuit. The resonances of coupled SIRs are tuned to match the transmission poles of a Chebyshev pass-band. By adding appropriate input/output coupling, the BPFs will have a quasi-Chebyshev response. Up to the present, the geometry in Fig. 2-1 of the SIRs with desired resonant spectrum can be obtained by the Eq. 2.1(odd mode) and Eq. 2.2(even mode). The center frequency of a triple-mode SIR is at its second resonance, while that of a dual-mode SIR is at the arithmetic mean of two resonances.

$$\tan \theta_1 = \times \cot \theta_2 \tag{2.1}$$

$$\cot \theta_1 = -R \times \tan \theta_2 \tag{2.2}$$

where $R = Z_2/Z_1$ is the impedance ratio and θ_1 and θ_2 are electrical lengths of the microstrip sections with characteristic impedances Z_1 and Z_2, respectively.
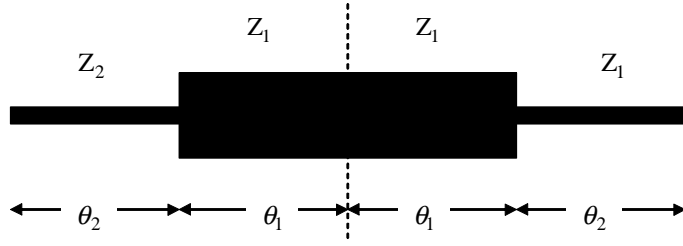
Figure 2-1: Geometry of a SIR with Z2>Z1

We calculate the corresponding resonant frequencies by the Eq. 2.3, 2.4, and 2.5. The insertion loss function of a kth-order Chebyshev filter can be expressed as

$$|S_{21}|^2 = 1 + \alpha |T_k(x)|^2 \tag{2.3}$$

where $T_k(x)$ is the kth-order Chebyshev polynomial of the first kind and α specifies the pass-band ripple level. The frequencies corresponding to $|x_n| = 0$ and 1 are center frequency and band edges, respectively. The kth-order poles in the equation are given as

$$x_n = \cos(\frac{2k + 1 - 2n}{2k}\pi), n = 1, 2, ..., k \tag{2.4}$$

For a kth-order Chebyshev BPF with fractional BW Δ, we can calculate the pole frequencies

$$\frac{f_n}{f_o} = 1 + x_n \times \frac{\Delta}{2} \tag{2.5}$$

where f_o is the center frequency.

Once we obtained the pole frequencies, the geometry of the SIR can be chosen to match the resonant frequencies with these transmission poles. It is assumed that I/O feeders do not shift the split-off frequencies significantly.

7

2.2 Design Procedure of Multimode Resonator Filter

Fig. 2-2 depicts the design flow chart of the MMR filters summarized from the above,
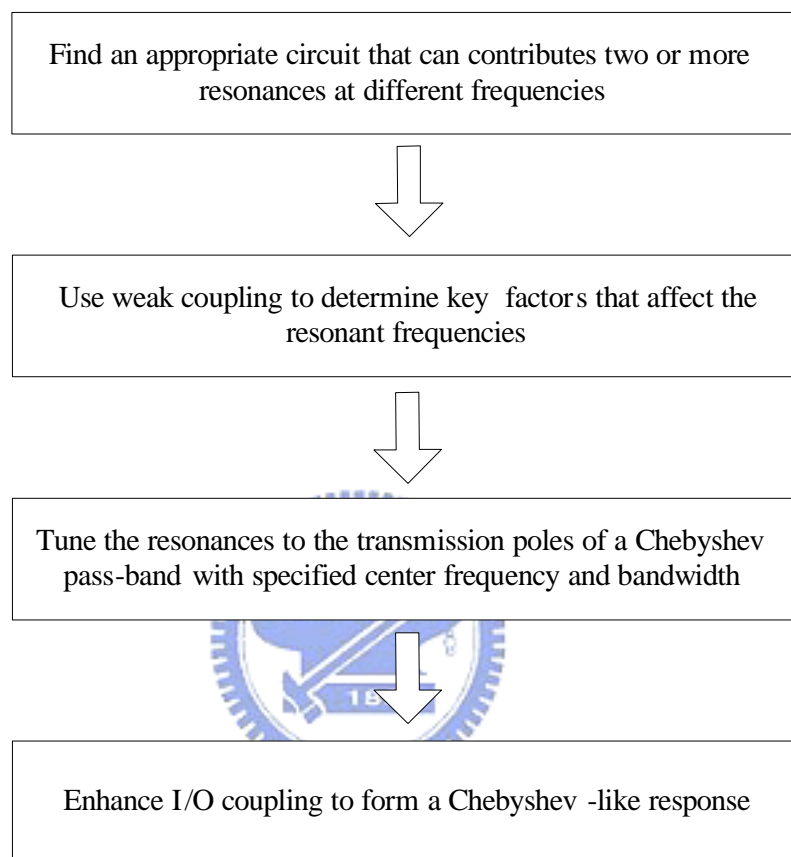
Figure 2-2: Design flow chart of MMR filters

Obviously, the design procedure mentioned above is very simple. That is why it wins acceptance among the filter design methods in the recent years. The first step is the most important. If we decide to use the framework that can not contribute resonances at desired frequencies or not easily be tuned by changing geometric parameter, it will lead to a failure in the end. Therefore we must choose our structure carefully. Next step is to find critical parameters that dominate the resonances. To ease the simulation, we should

fix some parameters and tune others to meet our goal, matching the resonances the transmission poles of a Chebyshev pass-band with specified center frequency and bandwidth. The last but not the least, adding appropriate input/output coupling structure, usually coupled lines, will construct the Chebyshev-like response with slight deviation form the Chebyshev poles. Eventually, the design is realized step by step. The rest of the work is to test and verify.

2.3   Proposed Multimode Resonator Filters

We start our research also according to the guidelines from the previous works. Firstly, we innovate a new structure which can be regarded as three parts- a $\lambda_c/2$(a half wavelength of center frequency) microstrip line in the middle, a $\lambda_z/4$(a quarter wavelength of transmission zero frequency) open-circuit stub, and a shunt reactance on the opposite side. The shunt reactance can be a short section of short-circuit stub, a patch capacitor, or a lumped circuit capacitor. The configuration of the circuit is like a cross. The idea comes from the T-shaped circuit with a $\lambda_c/2$ microstrip line in the middle and a $\lambda_c/4$ open-circuit stub. T-shaped circuit only has two resonances occurring nearby. Also, there were cross shaped networks with a $\lambda_c/2$ microstrip line in the middle and two $\lambda_c/4$ short-circuit stub on the opposite side that have been exploited before[10]. Whatever, two $\lambda_c/4$ microstrip line on the each side may occupy large space. As a result, it inspires us to create the design which has three resonances each adjoining to others and simultaneously reduces the size by using small short-circuit stub, patch, or lumped capacitor to replace the $\lambda_c/4$ stub.

Three kinds of tri-mode resonators are proposed. Each has three neighboring resonances and has a upper- or lower-stopband transmission zero. We regarded a small short-circuit stub as an shunt inductance leading to a transmission zero on upper-stopband. If we change the sign of the shunt reactance by replacing the short-circuit stub with a

capacitor, we can have a lower-stopband transmission zero. However, the frequency of the transmission zero is mainly decided by the electrical length of open-circuit stub.

In this paper, all circuits are implemented on a substrate with ε_r=3.58 and thickness=0.508 mm. Before the I/O coupling structure are equipped, the transmission poles are detected by a loose coupling scheme.

2.3.1 Tri-mode Resonator Filter with Upper-Stopband Transmission Zero

Fig. 2-3 shows the basic structure of the proposed resonator. Look deep into the structure, it can be sepapated into three resonators as depicted in Fig. 2-3. These three resonators contribute three distinct but adjacent resonant frequencies. Although, looking separately, three resonators have only two resonant frequencies, they are coupled to one another through the shunt reactance and the resonant frequencies are split into three frequencies. The filter described in this section has positive shunt reactance(inductive), $\lambda_z/4$ is electrically shorter than the three resonators. For the reason, the transmission zero's frequency, which is controlled by $\lambda_z/4$ open-circuit stub, falls above three resonant frequencies of the filter. That is, there is a transmission zero in the upper stop-band. An expression for the above discussion is presented in Fig. 2-4 and Fig. 2-5. On the other hand, if the reactance becomes negative(capacitive), the electrical lengths of the resonators are shorter than that of $\lambda_c/4$ and $\lambda_z/4$. And the transmission zero occurs in the lower stop-band instead. In this section, we use a small short-circuit stub to implement the shunt inductive reactance. It can be derived from the Eq. 2.6,

$$Z_{in} = jZ_0 \tan \beta l \tag{2.6}$$

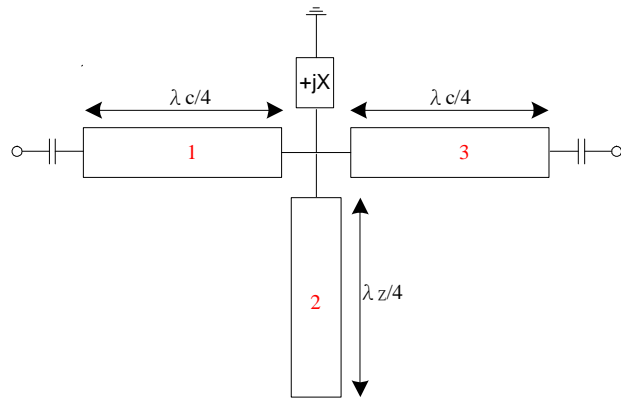where the length of short-circuit stub $l<\lambda/4$. The reactance is positive.

10

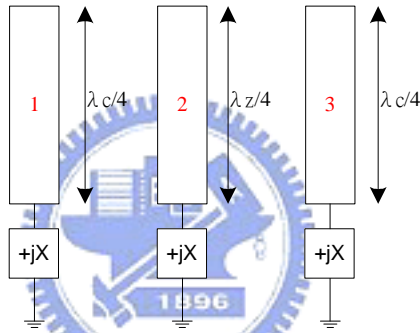Figure 2-3: Structure of tri-mode resonator with positive jX

Figure 2-4: Three resonators of tri-mode resonator with positive jX
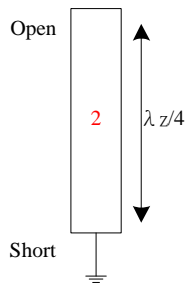
Figure 2-5: Zero controller of tri-mode resonator with positive jX

The filter in this thesis is different from the single SIR filter mentioned before. Our design has exactly three resonators, while the single SIR filter only has one resonator. SIR is trying to pull the second or third harmonic terms into the pass-band. The action has the possiblity that the spurious frequency may be pulled close to the pass-band at the same time unless there are special mechanisms for cancellation. However, the filter proposed here will have spurious frequency at almost three times above the center frequency.

After deciding the configuration, we use weak coupling to find the key factors. Simulation structure for tri-mode resonator with an upper stopband transmission zero at weak coupling condition is depicted in Fig. 2-6. Once we specify the center frequency and transmission zero frequency, we should have relative $\lambda_c/4$ and $\lambda_z/4$. For simplifying the design, we fix impedance of $\lambda_c/4$ transmission lines to be 50Ω which matches the port impedance. Then, the parameters Z_{open}(impedance of open-circuit stub), Z_{short}(impedance of short-circuit stub), and θ_{short}(length of short-circuit stub) are the parameters which should be found out. Fig. 2-7, 2-8, and 2-9 indicate the parameters effects on resonant frequencies- f_1, f_0, and f_2, which are named by frequencies from low to high. Hoping to find out some useful information, we analysis these figures in detail. Firstly, f_0 is almost fixed at center frequency of 2.45 GHz in spite of the changing in Z_{open}, Z_{short}, and θ_{short}. It seems that f_0 is principally decided by two $\lambda_c/4$ microstrip line. In addition, f_z is controlled by the $\lambda_z/4$ open-circuit stub and locate exactly where we desired. Secondly, Z_{open} affects f_1 and f_2 almost with the same degree, while Z_{short} and θ_{short} have more impact on f_1 and less on f_2.

Figure 2-6: Simulated schematic circuit with loose coupling in AWR

Figure 2-7: Effect of the impedance of short-circuit stub(Z_{short}) on resonant frequencies

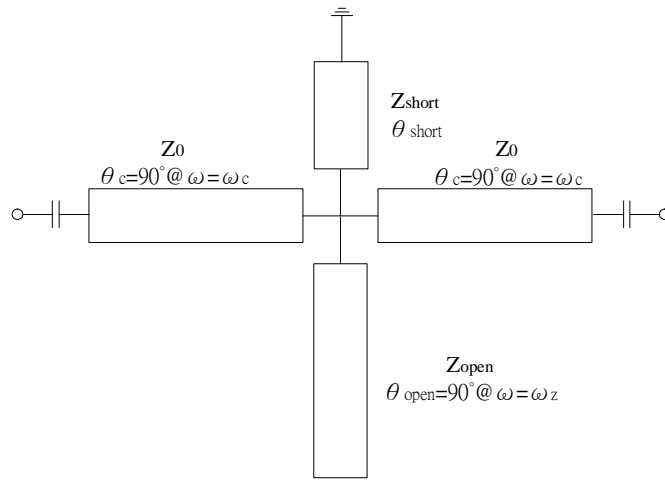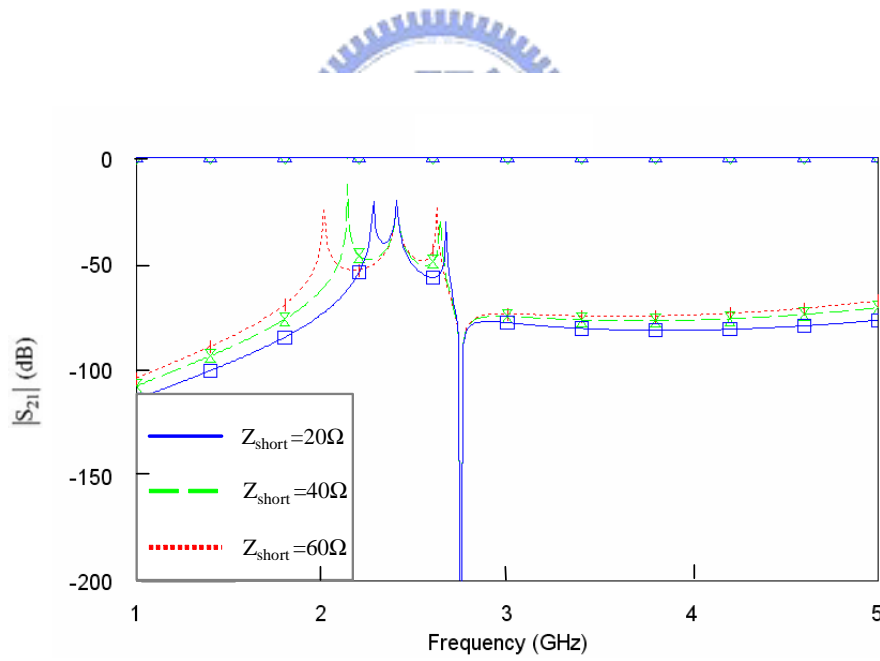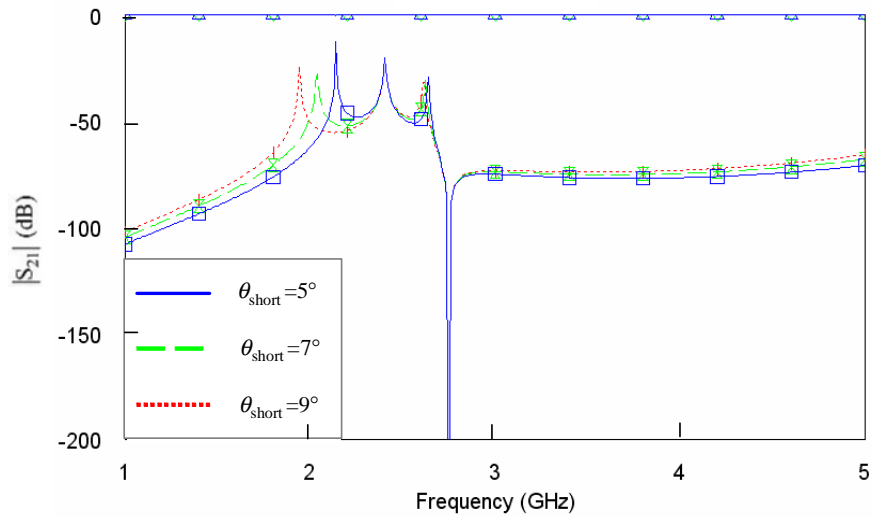Figure 2-8: Effect of the length of short-citcuit stub(θ_{short}) on resonant frequencies
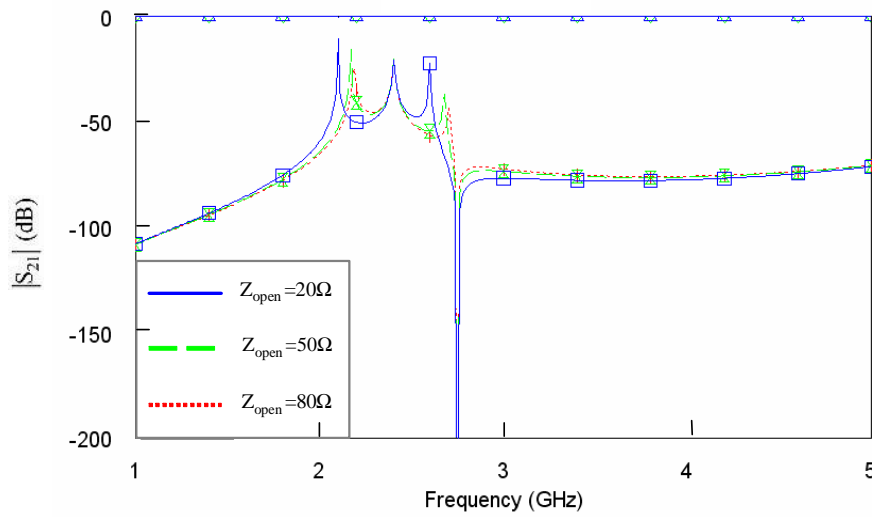

Figure 2-9: Effect of the impedance of open-circuit stub(Z_{open}) on resonant frequencies

The results are very helpful to our simulation. Once the center frequency and bandwidth is given, we can compute corresponding Chebyshev pole frequencies and use two $\lambda_c/4$ microstrip lines in the middle to fix f_0. Next, we set the transmission zero frequency by changing the length open-circuit stub. Then, Z_{open} must to be decided before others, because Z_{short} and θ_{short} influence f_2 less. In other word, we match the f_2 to the pole of Chebyshev response first. Afterwards, we change Z_{short} and θ_{short} to tune f_1 to meet the pole frequency. To this step, the filter is fundamentally achieved. But we still need to add coupled lines at input/output stage to transform the above response to a Chebyshev band-pass response.

Both simulation and measurement of the 2.45 GHz multiple-mode resonator filter with bandwidth Δ=20% are presented as follows. We calculate the corresponding resonant frequencies by the Eqs. 2.3, 2.4, and 2.5 , and then we have Chebyshev pole frequencies at $f_1 = 2.18\text{GHz}$, $f_0 = 2.45\text{GHz}$, and $f_2 = 2.62\text{GHz}$ separately. Next step is to match the pole frequencies. Since the center resonant frequency f_0 has been set by two $\lambda_c/4$ microstrip lines in the middle. We only need to tune Z_{open} to match f_2 of the circuit to 2.62GHz, and then adjust Z_{short} and θ_{short} to match f_1 of the circuit to 2.18GHz.

Fig. 2-10 and Fig. 2-11 are the simulated circuit schematic and result in AWR(circuit simulation) where Fig. 2-12 and Fig. 2-13 are the simulated physical layout and result in Sonnet(EM simulation). One thing needs to be noticed is that we bend the coupled line stage to reduce the area of the circuit. We adjust length of the coupled line at the same time. The simulated result of the bended filter still shows good agreement with the original one, and we expect the measurement result will coincide with the simulaton result as well. A photograph of the fabricated filter is given in Fig. 2-14. Fig. 2-15 and Fig. 2-16 plot measured performance in narrow band(1GHz~5GHz) and wide band(1GHz~8GHz), respectively. We can foresee that the spurious frequency will occur at three times above the center frequency.
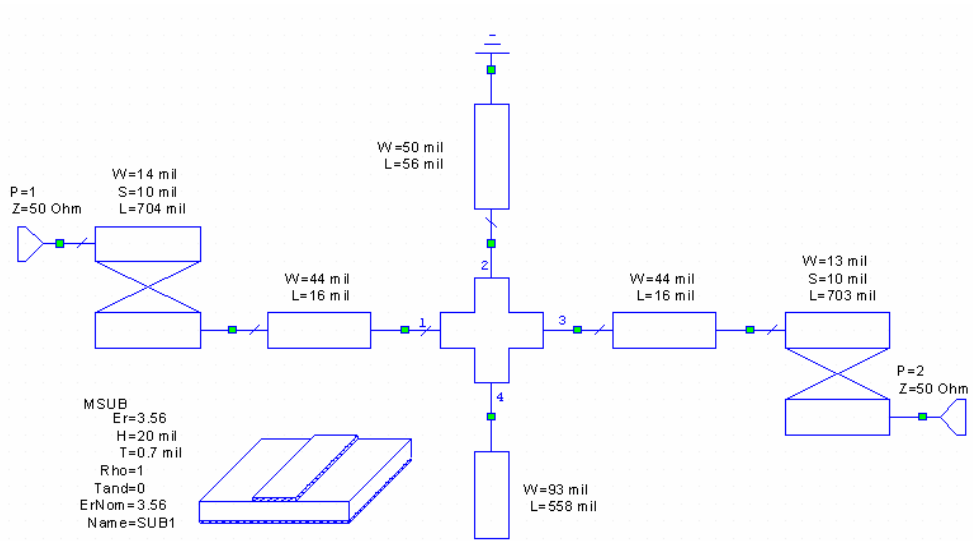
Figure 2-10: Simulated schematic circuit of tri-mode filter with an upper-stopband transmission zero in AWR
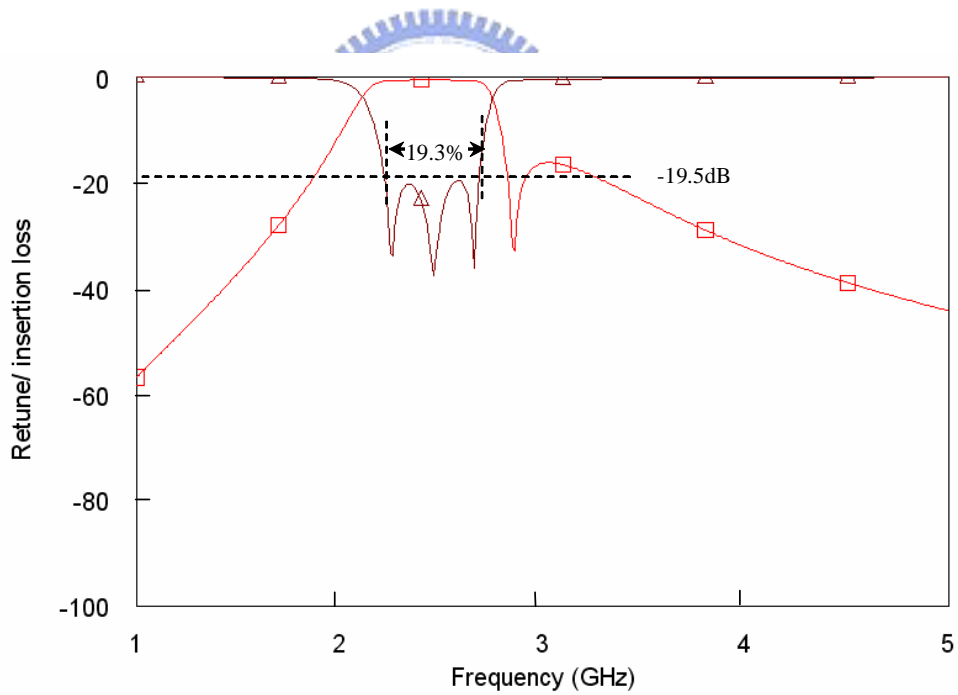
Figure 2-11: Simulated frequency response of tri-mode filter with an upper-stopband transmission zero in AWR
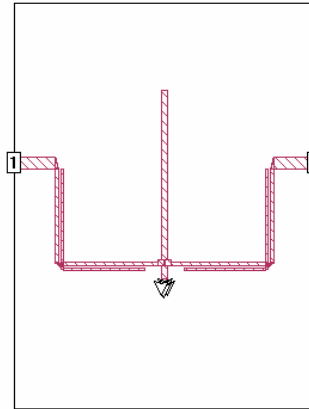
Figure 2-12: Simulated physical layout of tri-mode filter with an upper-stopband transmission zero in Sonnet
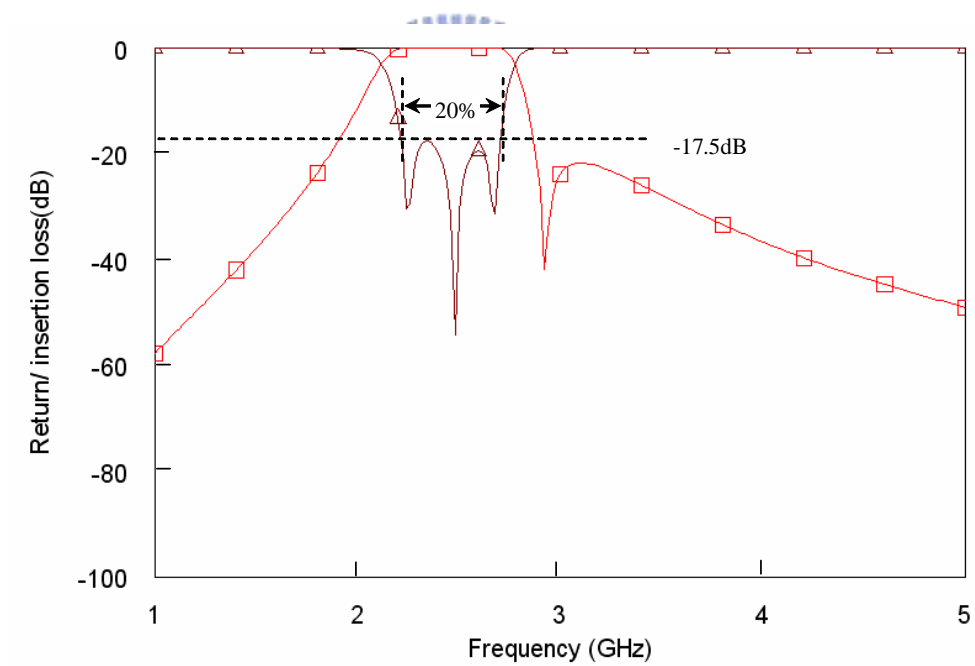
Figure 2-13: Simulated frequency response of tri-mode filter with an upper-stopband transmission zero in Sonnet

17
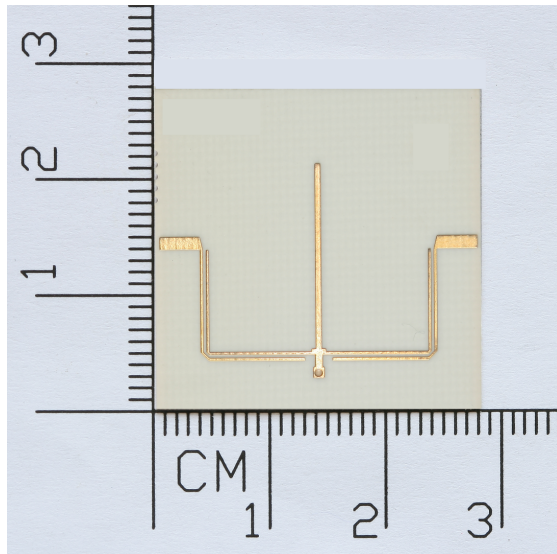
Figure 2-14: Photograph of tri-mode filter with an upper-stopband transmission zero
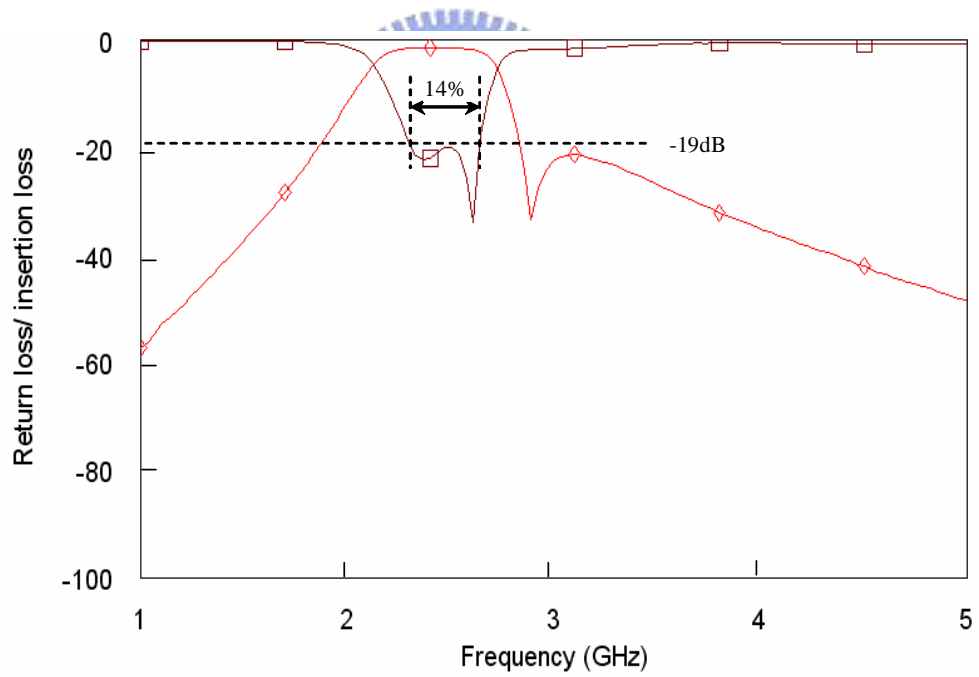
Figure 2-15: Measured frequency response of tri-mode filter with an upper-stopband transmission zero(narrow band)
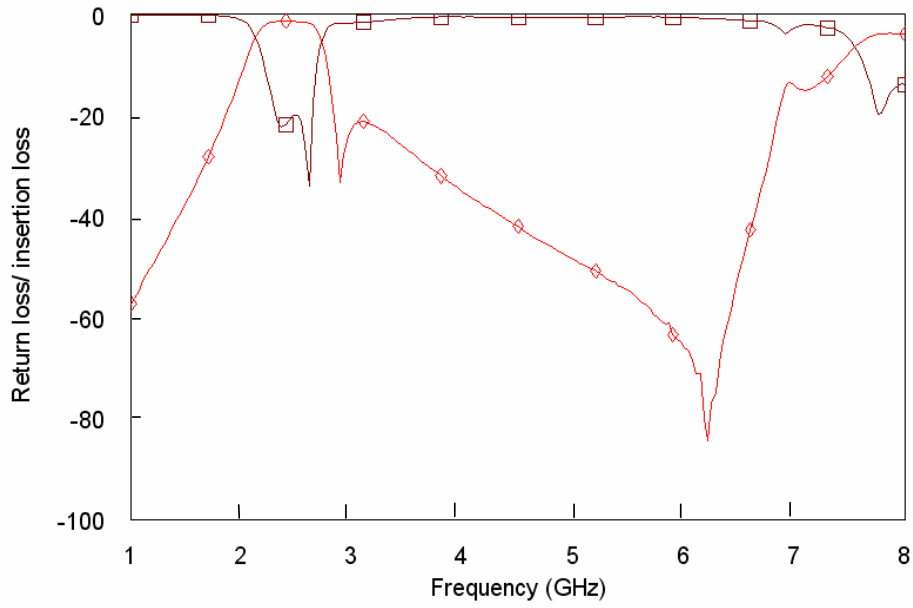
Figure 2-16: Measured frequency response of tri-mode filter with an upper-stopband transmission zero(wide band)

The measured data shows that the in-band insertion loss is 1.43dB and the return loss is 19dB. Comparing to the simulation, the response with slightly shrunk bandwidth $\Delta=14\%$ agree with the simulation reasonably. Spurious frequency locates near 7.35GHz as we foretold before. It convinces us that the structure and the design rules for multi-mode resonator function well. And then, we can try to move the transmission zero to the lower side of the pass-band, whereas the previous filter has the transmission zero on the higher side. We will see the design of triple-mode resonator filter with a lower-stopband transmission zero in the next subsection, and validate with the experiment.

2.3.2 Tri-mode Resonator Filter with Lower-Stopband Transmission Zero

Based on experience of the triple-mode resonator filters in previous section, we suggest that triple-mode resonator filters with a lower-stopband transmission zero can also be synthesized easily. As we predicted before, the negative reactance leads to that $\lambda_z/4$ microstrip line is going to be electrically longer than any of the resonators. It must be emphasized that the length of the open-circuit stub must be longer than the previous design. The relations between resonators are depicted in Fig. 2-17 and Fig. 2-18, and Fig. 2-19. Apparently, there is a transmission zero in the lower stop-band. A shunt capacitive reactance is used to represent $-jX$ here. We try both lumped and distributed capacitor in this section.
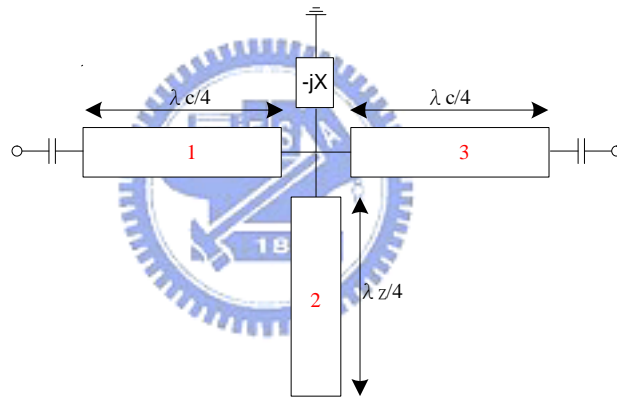
Figure 2-17: Structure of tri-mode resonator filter with negative jX
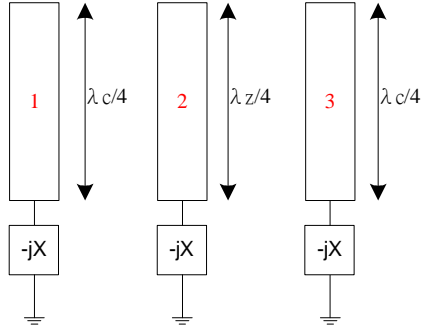
Figure 2-18: Three resonators of tri-mode resonator filter with negative jX
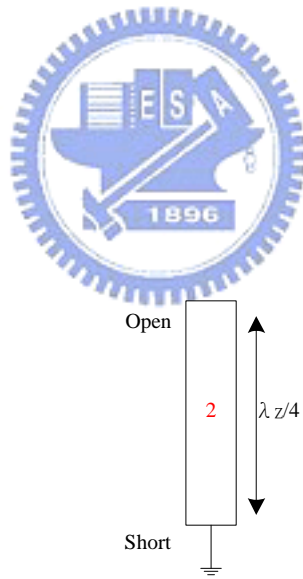
Figure 2-19: Zero controller of tri-mode resonator filter with negative jX

Follow the same procedure, we must find out the key parameters of the triple-mode resonator filters with a lower stopband transmission zero. We will have $\lambda_c/4$ and $\lambda_z/4$ correspond to the specified center frequency and zero frequency, respectively. Simulation with loose external coupling is depicted in Fig. 2-20. To simplify the simulation, we fix impedance of $\lambda_c/4$ transmission lines to be 50Ω which matches the port impedance of the system. Then, the parameters Z_{open}(impedance of open-circuit stub) and C are left to be designed. Fig. 2-21 and Fig. 2-22 indicate the parameters correspond to resonant frequencies- f_1, f_0, and f_2 ,which are named by frequencies from low to high. We extract the information from the comparison. First, f_0 keep still at center frequency of 2.45 GHz despite of the changing in Z_{open} and C. It seems that f_0 is principally decided by two $\lambda_c/4$ microstrip line. In addition, f_z is controlled by the $\lambda_z/4$ open-circuit stub and located exactly where we designated. Z_{open} affects f_1 and f_2 at the same time while C have more influences on f_2 and less on f_1.
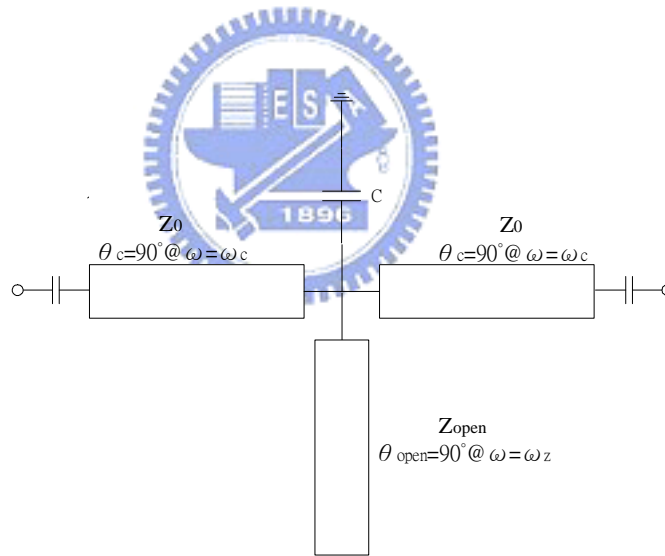
Figure 2-20: Simulated schematic circuit with loose coupling in AWR
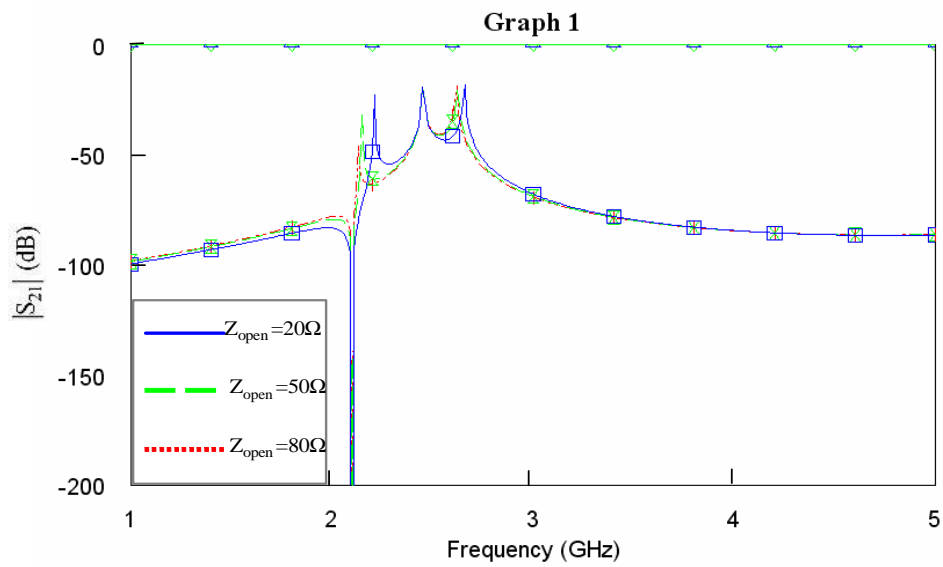
Figure 2-21: Effect of the impedance of open-circuit stub(Z_{open}) on resonant frequencies
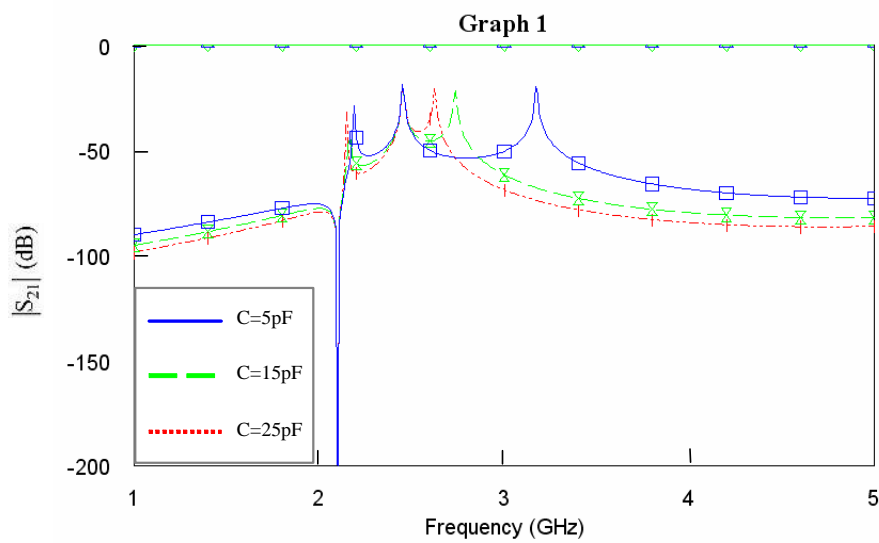
Figure 2-22: Effect of capacitor(C) on resonant frequencies

We collect these useful informations. Once the center frequency and bandwidth is given, we can compute corresponding Chebyshev pole frequencies. We lay two $\lambda_c/4$ microstrip lines in the middle to fix the f_0. Next, we set the transmission zero frequency by changing the length of open-circuit stub. Then, Z_{open} must to be decided before others, because C influences f_1 less. In other word, we match the f_1 to the pole of Chebyshev response first. Afterwards, we change C for tuning f_2 to meet the pole frequency. To this step, the filter design is fundamentally achieved. But we still need to add coupled lines at input/output stage to transform the above response to a Chebyshev band-pass response.

Both simulation and measurement of the 2.45 GHz multiple-mode resonator filter with bandwidth $\Delta=20\%$ are presented as follows. We calculate the corresponding resonant frequencies by the Eqs. 2.3, 2.4, and 2.5, and then we have Chebyshev pole frequencies at $f_1=2.18$GHz, $f_0=2.45$GHz, and $f_2=2.62$GHz separately. Next step is to match the pole frequencies. Since the center resonant frequency has been set by two $\lambda_c/4$ microstrip lines in the middle. We only need to tune Z_{open} to match f_1 of the circuit to 2.18GHz, and then adjust C to match f_2 of the circuit to 2.62GHz.

Fig. 2-23 and Fig. 2-24 are the simulated schematic circuit and results in AWR(circuit simulation). Since lumped capacitor cannot be simulated in EM simulator, we fabricate the filter directly without EM simulation. One thing needs to be noticed is that we bend the coupled line stage to reduce the area of the circuit. We adjust length of the coupled line at the same time to make sure the performance unchanged. Fig. 2-25 depict the photogragh of the circuit. Fig. 2-26 and Fig. 2-27 plot measured performance in narrow band(1GHz~5GHz) and in wide band(1GHz~8GHz). We can foresee that the spurious frequency will occur at three times above the center frequency.
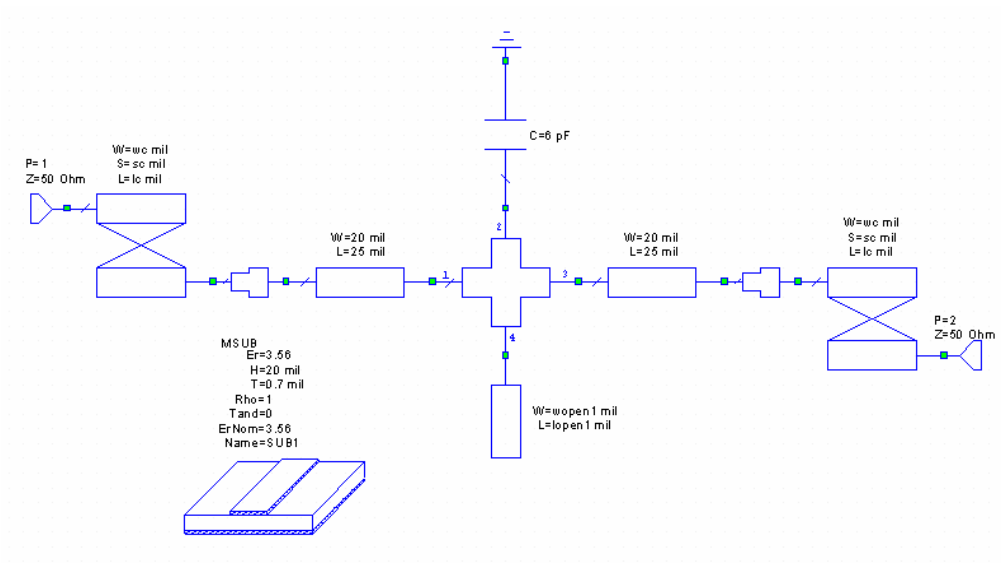
Figure 2-23: Simulated schematic circuit of tri-mode filter with strong coupling with a lower-stopband transmission zero in AWR
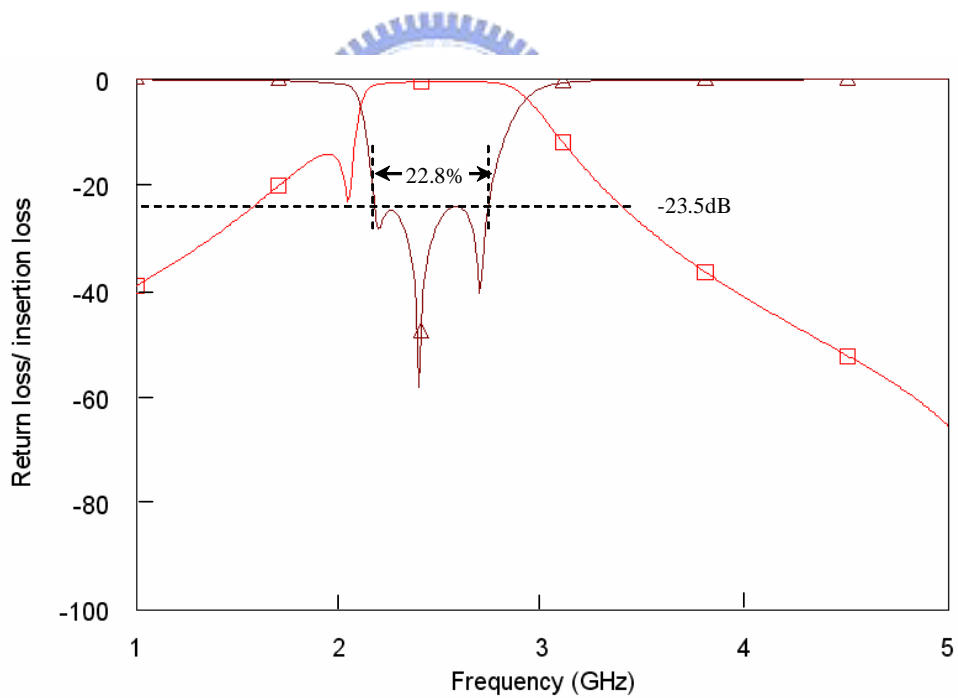
Figure 2-24: Simulated frequency response of tri-mode filter with a lower-stopband transmission zero in AWR

25

Figure 2-25: Photograph of the tri-mode filter with a lower-stopband transmission zero using a lumped capacitor

Figure 2-26: Measured frequency response of tri-mode filter with a lower-stopband transmission zero using a lumped capacitor (narrow band)

Figure 2-27: Measured frequency response of tri-mode filter with a lower-stopband transmission zero using a lumped capacitor(wide band)

The measured data shows that the in-band insertion loss is 0.9dB and the return loss is 19dB.When we implement the filter at high frequency with lumped capacitor, there is a problem about value change of the capacitance. As we can see from the above figures, the measured bandwidth Δ=30.8% is much larger than simulated one Δ=22.8%. The variation of the capacitance is unpredictable. We have to try several capacitors of different values to approximate the simulated performance. The capacitor chosen finally is 1.8PF rather than 4.8PF used in simulation. The reason of the capacitance value drift is mainly due to the parasitic inductance of the chip capacitor. Because the equivalent circuit of this chip capacitor is unknown, the value change is unpedictable. The bandwidth of the filter varies with the parasitic inductance.

To eliminate the problem, we bring up the idea to replace lumped capacitor with distributed capacitor(patch capacitor). The physical layout and simulated result in Sonnet have presented in Fig. 2-28 and Fig. 2-29. A photograph of the fabricated filter is given in Fig. 2-30. We also depicted the measured data in Fig. 2-31 for narrow band(1GHz~5GHz) and Fig. 2-32 for wide band(1GHz~8GHz). Evidently, the measured and the simulated performance matches much better than the previous one. This is a good information for the designer, since the characteristic of the circuit can be well-described.
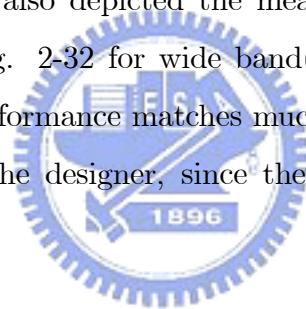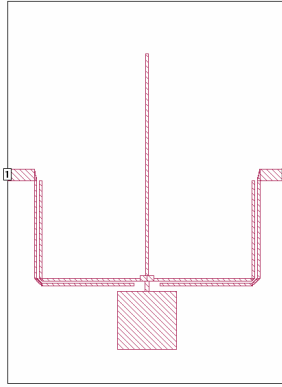
Figure 2-28: Simulated physical layout of tri-mode filter with a lower-stopband transmission zero using a patch capacitor in Sonnet
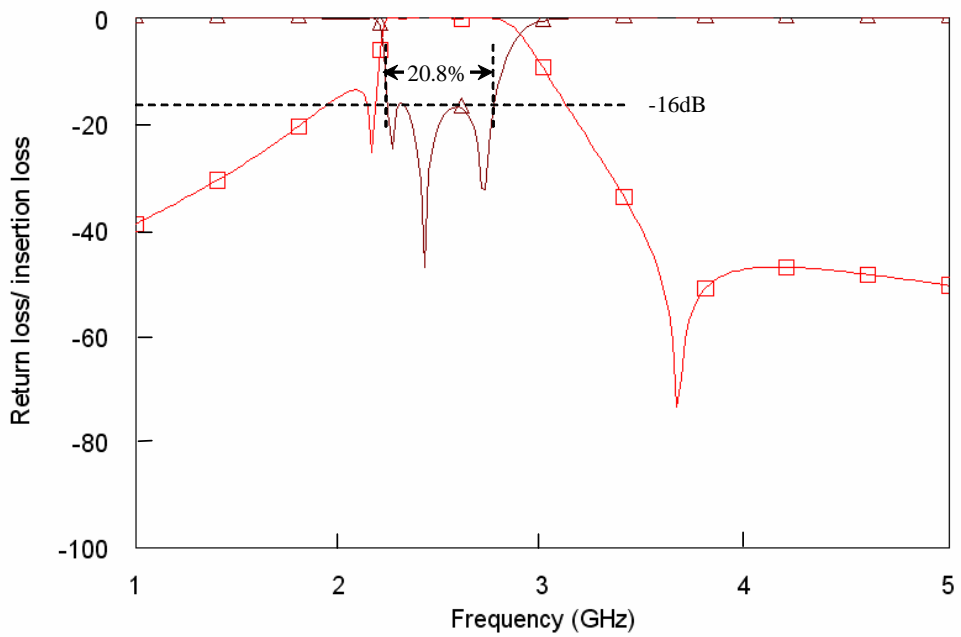
Figure 2-29: Simulated frequency response of tri-mode filter with a lower-stopband transmission zero using a patch capacitor in Sonnet
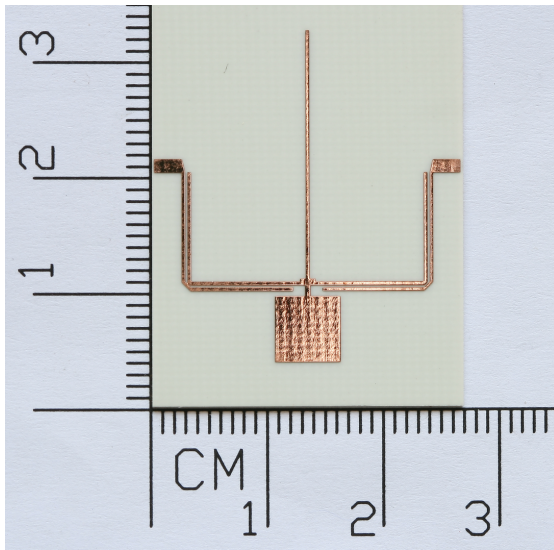
Figure 2-30: Photograph of the tri-mode filter with a lower-stopband transmission zero using a patch capacitor
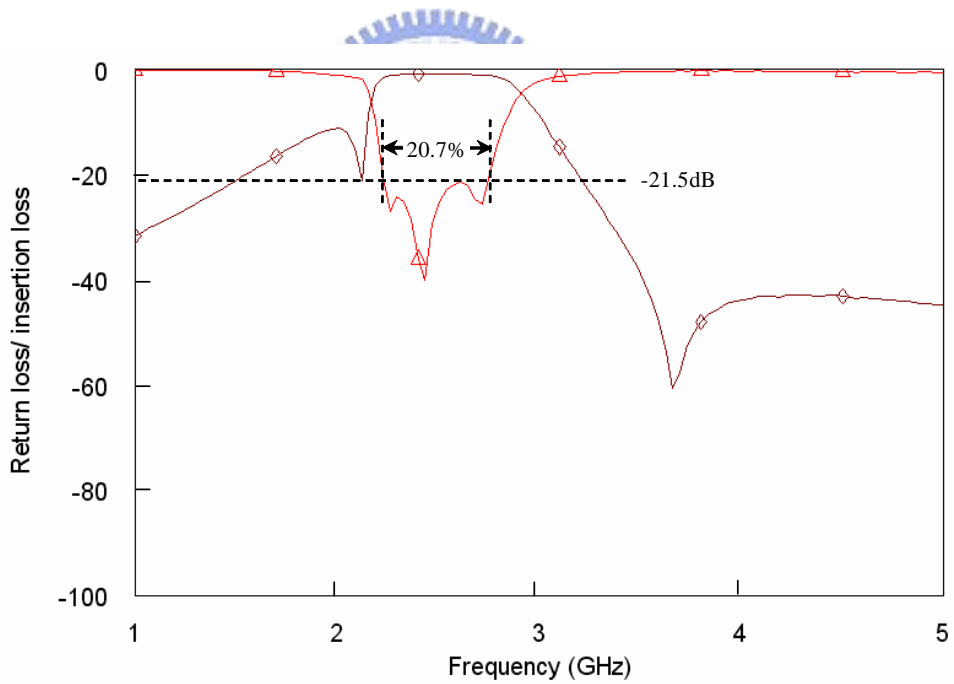
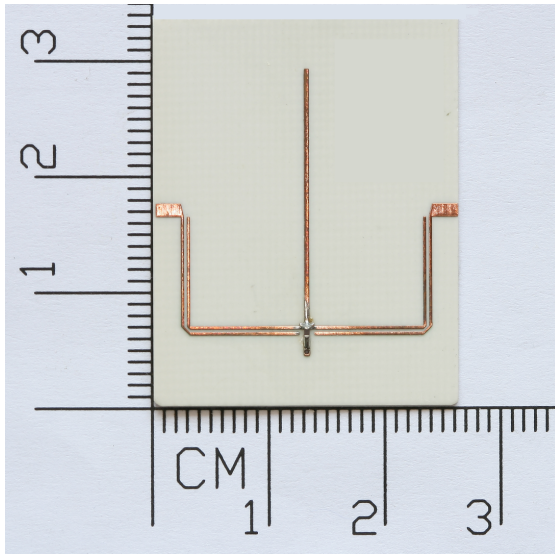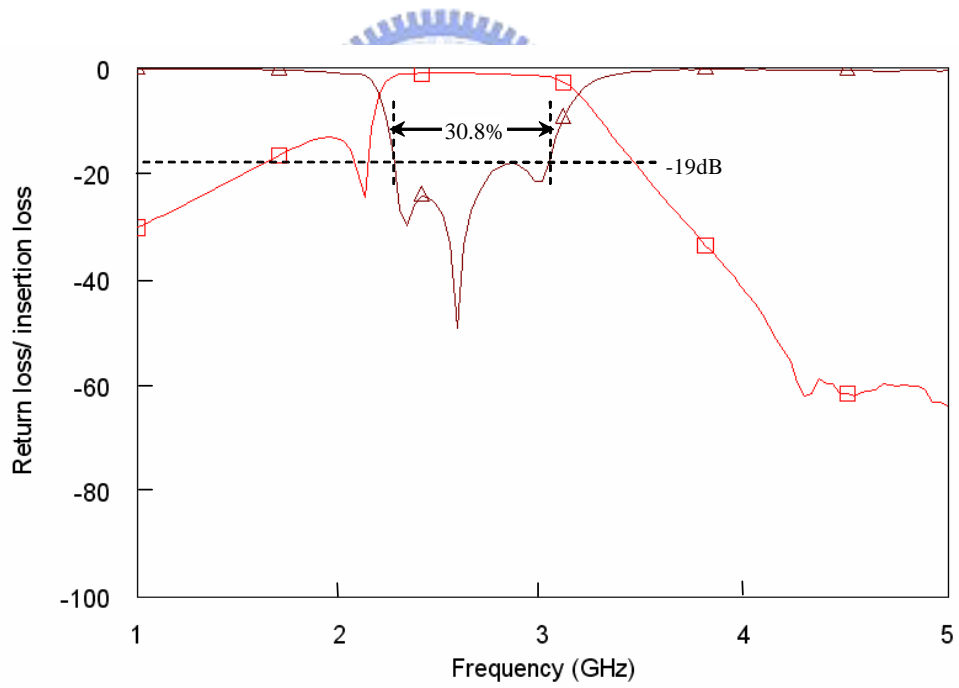Figure 2-31: Measured frequency response of tri-mode filter with a lower-stopband transmission zero using a patch capacitor(narrow band)
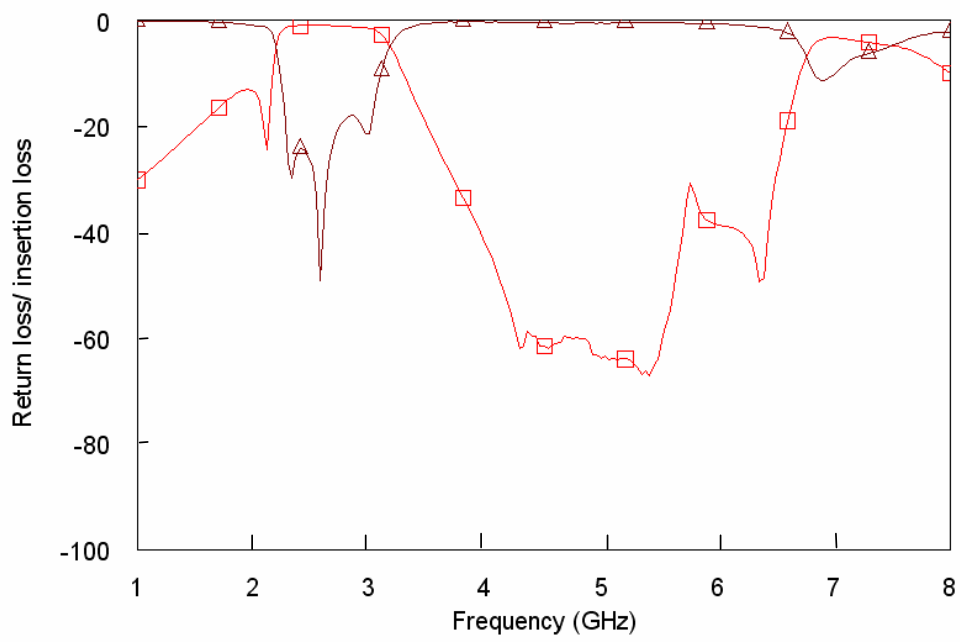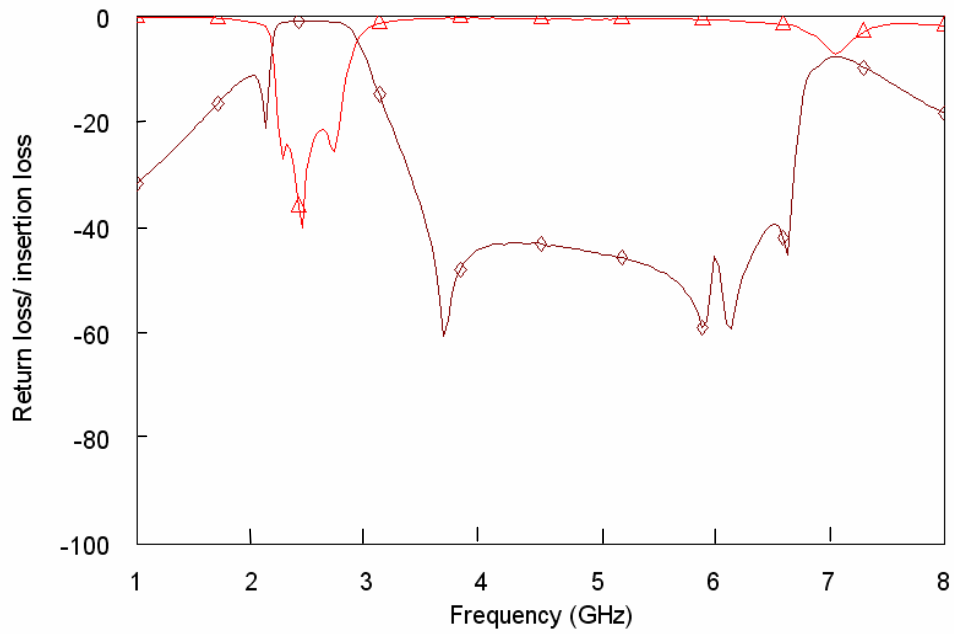
Figure 2-32: Measured frequency response of tri-mode filter with a lower-stopband transmission zero using a patch capacitor(wide band)

The measured data shows that the in-band insertion loss is 0.9dB and the return loss is 21.5dB. The measured bandwidth Δ=20.7% is almost consistent with the simulated one Δ=20.8%. The experiment verifies that the capacitor implemented by distributed element is more reliable than the one implemented by lumped element, especially in high frequency band.

2.3.3 Comparison of the Filter with Upper-Stopband Transmission Zero and the Filter with Lower-Stopband Transmission Zero

There is an interesting topic here. The rejection ability of the filter with upper-stopband transmission zero and the filter with lower-stopband transmission zero at frequency near dc are quite different. This is reasonable because the tri-mode filter with an upper-stopband transmission zero is naturally a third order filter at low frequency. Two coupled line stages together with small short-circuit stub in the middle of $\lambda_c/2$ microstrip line reject low frequency signal significantly. However, the tri-mode filter with a lower-stopband transmission zero only has two coupled line stages to suppress low frequency signal, which can be considered a two order filter at low frequency. We can easily verify our prediction by demonstrate the contract between Fig. 2-33 and Fig. 2-34. Obviously, the insertion loss of the filter with an upper stopband transmission zero near dc is approaching 100dB, while the insertion loss of the filter with a lower stopband transmission zero near dc is approaching 60dB. In conclusion, the excellent low rejection ability of the low frequency signal is an attractive advantage of the proposed tri-mode filter with an upper stopband transmission zero.
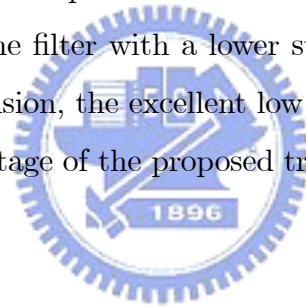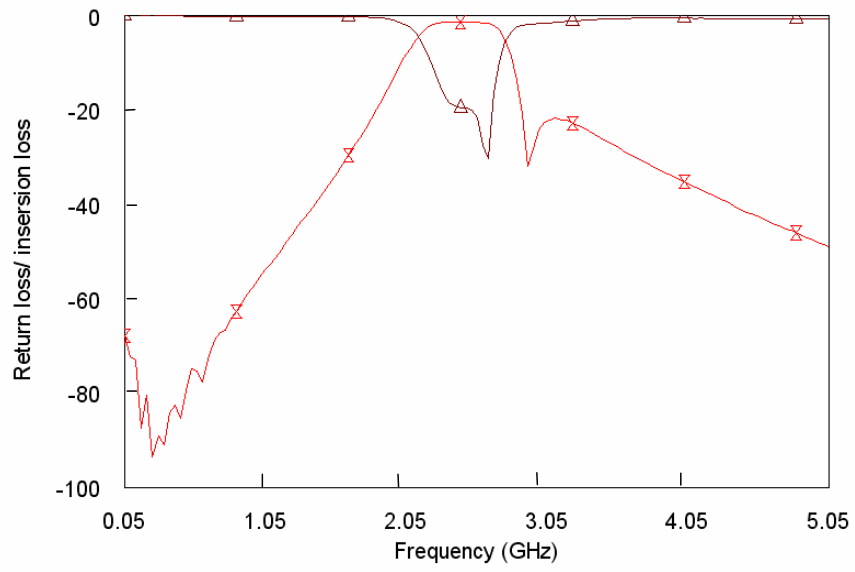
Figure 2-33: Low stop-band rejection ability of the tri-mode filter with an upper-stopband transmission zero
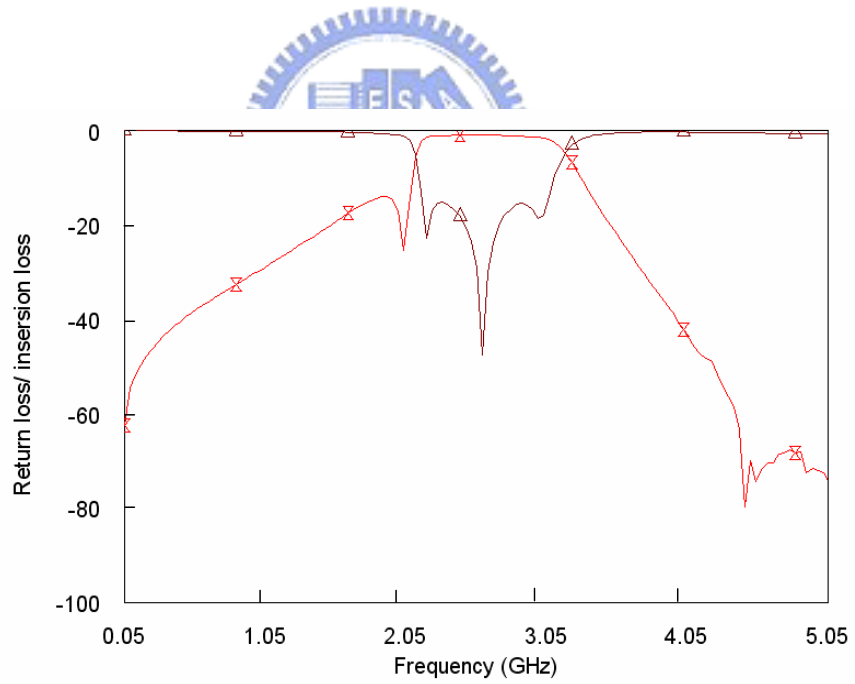
Figure 2-34: Low stop-band rejection ability of the tri-mode filter with a lower-stopband transmission zero

33

Chapter 3

J and K Inverter Filters

3.1 Filters with Ideal J and K inverters

3.1.1 Low-pass Prototype Filter

The element value g_0, g_1, g_2,......, g_n, g_{n+1} of th low-pass prototype filters discussed in this chapter are defined as shown in Fig. 3-1(a) or (b). Either form has identical responses. The following conversions in Fig. 3-2 are observed:
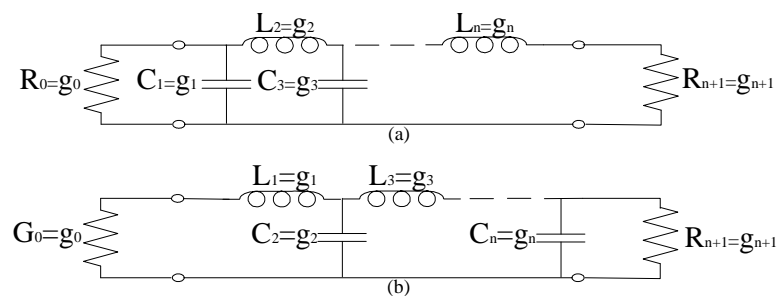
Figure 3-1: Low-pass prototype

$$g_k\big|_{k=1\sim n} = \begin{cases} \text{the inductance of a series coil} \\ \text{the capacitance of a shunt capacitor} \end{cases}$$

$$g_0 = \begin{cases} \text{the generator resistance } R_0 \text{ if } g_1=C_1 \\ \text{the generator conductance } G_0 \text{ if } g_1=L_1 \end{cases}$$

$$g_{n+1} = \begin{cases} \text{the load resistance } R_{n+1} \text{ if } g_n=C_n \\ \text{the load conductance } G_{n+1} \text{ if } g_n=L_n \end{cases}$$

Figure 3-2: Definition of g_k

The circuit element values, g_k, can be looked up in the tables with given specification(pass-band ripple level and filter order n). Fig. 3-3 is the table for the g_k of Chebyshev reponse with pass-band ripple level =0.01dB and filter order from 1 to 10.

Value of n	g_1	g_2	g_3	g_4	g_5	g_6	g_7	g_8	g_9	g_{10}	g_{11}
0.01dB ripple											
1	0.0960	1.0000									
2	0.4488	0.4077	1.1007								
3	0.6291	0.9702	0.6291	1.0000							
4	0.7128	1.2003	1.3212	0.6476	1.1007						
5	0.7563	1.3049	1.5773	1.3049	0.7563	1.0000					
6	0.7813	1.3600	1.6896	1.5350	1.4970	0.7098	1.1007				
7	0.7969	0.3924	1.7481	1.6331	1.7481	1.3924	0.7969	1.0000			
8	0.8072	0.4130	1.7824	1.6833	1.8529	1.6193	1.5554	0.7333	1.1007		
9	0.8144	1.4270	1.8043	1.7125	1.9057	1.7125	1.8043	1.4270	0.8144	1.0000	
10	0.8196	1.4369	1.8192	1.7311	1.9362	1.7590	1.9055	1.6527	1.5817	0.7446	1.1007

Figure 3-3: The g_k of Chebyshev reponse with pass-band ripple level =0.01dB

As we mentioned before, J and K inverters can convert the filter to all series or all shunt elements. Fig. 3-1 is the example of using K inverter to change shunt capacitors in Fig. 3-4 to series inductors, that is, we change the network to all series elements.
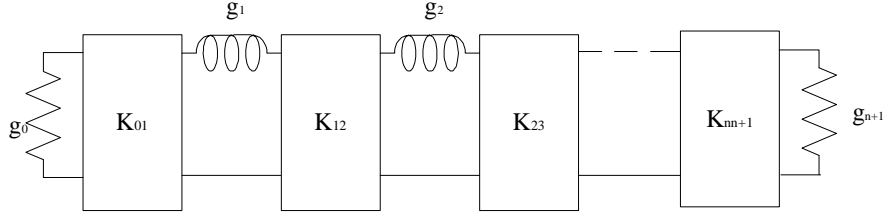
Figure 3-4: Using K inverter to change shunt capacitors to series inductors

3.1.2   Low-pass Prototype Filter to Band-pass Filter Transformation

The low-pass prototype filter in the previous section can be transformed to band-pass filter through frequency transformation as shown in Eq. 3.1.

$$\frac{\Omega}{\Omega_c} = \frac{1}{\Delta}(\frac{\omega}{\omega_0} - \frac{\omega_0}{\omega}) \tag{3.1}$$

where $\omega_0=2\pi f_0$ (f_0 is the center frequency of the pass-band), $\Delta=\frac{(\omega_2-\omega_1)}{\omega_0}$($\Delta$ is the fractional bandwidth of the band-pass filter), and $\Omega_c=1$ (Ω_c is the cutoff frequency of the low-pass prototype filter). Then, we have

$$jX_k = j\frac{\Omega}{\Omega_c} \times g_k = j\frac{1}{\Delta}(\frac{\omega}{\omega_0} - \frac{\omega_0}{\omega}) \times g_k = j\omega L_k + \frac{1}{j\omega C_k} \tag{3.2}$$

where $L_k=\frac{g_k}{(\Delta\times\omega_0)}$, $C_k =\frac{\Delta}{(\omega_0\times g_k)}$, and $x_k=\frac{\omega_0}{2}\frac{dX_k}{d\omega}|_{\omega=\omega_0} = \omega_0 L_k$($x_k$ is the reactance slope parameter of the resonator k). The band-pass after transformation is depicted in Fig. 3-5.
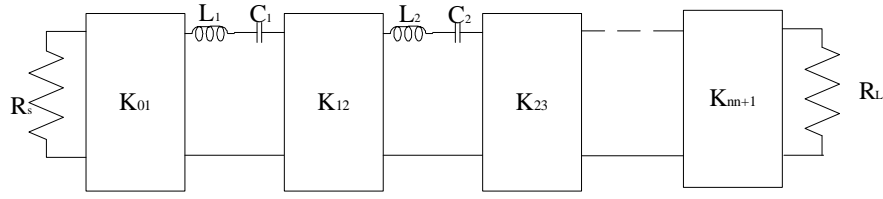
Figure 3-5: Transform LPF to BPF

We can also obtain the equations as follows:

$$K_{01} = \sqrt{\frac{x_0 R_s}{g_0 g_1} \times \Delta} \tag{3.3}$$

$$K_{nn+1} = \sqrt{\frac{x_n R_L}{g_n g_{n+1}} \times \Delta} \tag{3.4}$$

$$K_{kk+1} = \sqrt{\frac{x_k x_{k+1}}{g_k g_{k+1}}} \times \Delta, k = 1, 2, ..., n-1 \tag{3.5}$$

where R_s is the source resistance and R_L is the load resistance. Follow the same rules, we can also write the equations for J inverter.

$$J_{01} = \sqrt{\frac{b_1 G_s}{g_0 g_1} \times \Delta} \tag{3.6}$$

$$J_{nn+1} = \sqrt{\frac{b_n G_L}{g_n g_{n+1}} \times \Delta} \tag{3.7}$$

$$J_{kk+1} = \sqrt{\frac{b_k b_{k+1}}{g_k g_{k+1}}} \times \Delta, k = 1, 2, ..., n-1 \tag{3.8}$$

where G_s is the source admittance and G_L is the load admittance. Follow the same rules, we can also write the equations for J inverter.

3.2 Symmetric J and K Inverter Filters

As we mentioned before, J and K inverters can convert the filter to all series or all shunt elements. It can be seen as a quarter-wavelength transformer. A quarter-wavelength transformer can only contribute $-90°$ delay at center frequency, while J and K inverter can have $+90°$ or $-90°$ delays. And the delays providing by J and K inverters are invariant over the whole spectrum. Evidently, the J and K inverters do not exist in real world. As a result, we usually find equivalent circuit around the center frequency of the band-pass filter. Also, it is hard to implement wide bandwidth BPFs by using J or K inverters. However, it is a good design method for narrow to moderate bandwidth filters. We can find equivalent networks for J and K inverters by letting ABCD matrices equal at the certain frequency. Fig. 3-7 and Fig. 3-8 are the examples for K and J inverters implementation, respectively. Inverters of this kind are suitable in transmission lines filter, because the $\psi/2$ transmission lines with characteristic impedance Z_0 can be embedded into transmission line resonators.
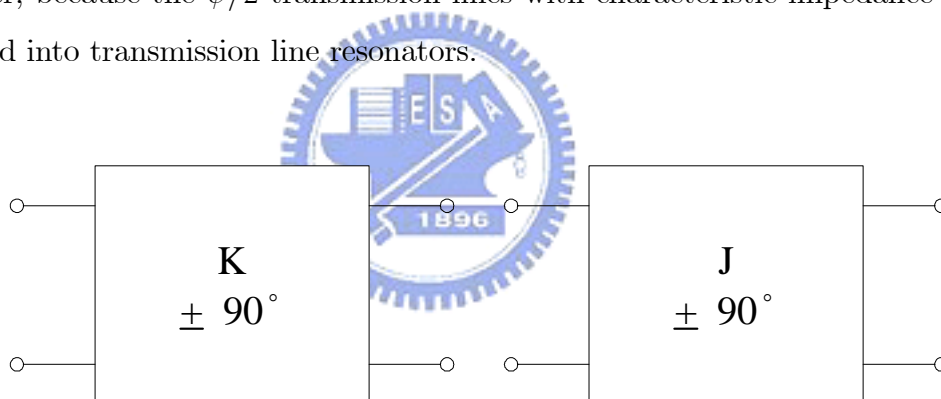
Figure 3-6: J and K inverters
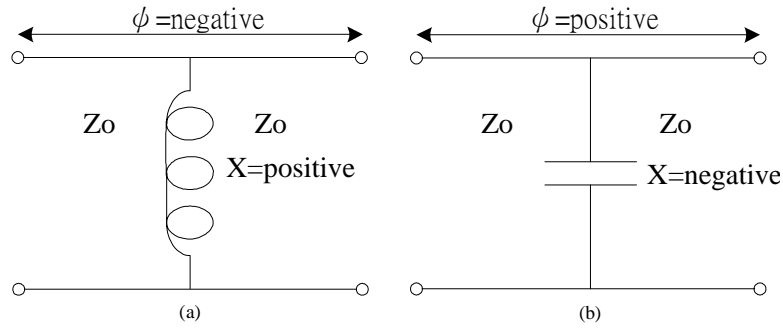
Figure 3-7: K inverters implementation with equal impedance transmission lines besides the shunt reactance
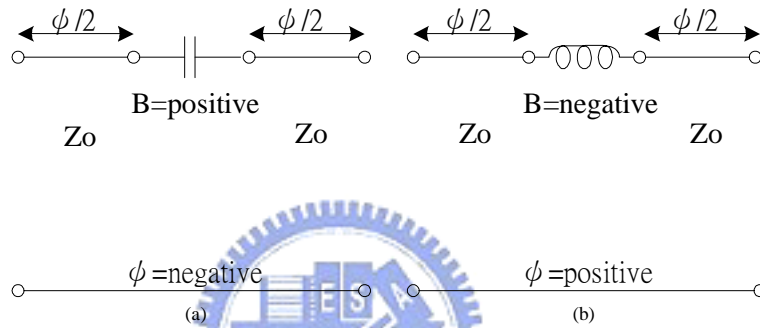
Figure 3-8: J inverters implementation with equal impedance transmission lines besides the series susceptance

We can match Fig. 3-7 to K inverter and Fig. 3-8 to J inverter by equalizing the ABCD matrices. The ABCD matrix of K inverter and J inverter are

$$
\begin{pmatrix} A & B \\ C & D \end{pmatrix} = \begin{pmatrix} 0 & \pm jK \\ \pm j\frac{1}{K} & 0 \end{pmatrix}, \begin{cases} (+)when + 90° \\ (-)when - 90° \end{cases}
\tag{3.9}
$$

$$
\begin{pmatrix} A & B \\ C & D \end{pmatrix} = \begin{pmatrix} 0 & \pm j\frac{1}{J} \\ \pm jJ & 0 \end{pmatrix}, \begin{cases} (+)when + 90° \\ (-)when - 90° \end{cases}
\tag{3.10}
$$

39

The ABCD matrix of Fig. 3-7 and Fig. 3-8 are

$$
\begin{pmatrix} A & B \\ C & D \end{pmatrix} = \begin{pmatrix} \cos\left(\frac{\psi}{2}\right) & \frac{j\sin\left(\frac{\psi}{2}\right)}{Y_0} \\ jY_0\sin\left(\frac{\psi}{2}\right) & \cos\left(\frac{\psi}{2}\right) \end{pmatrix} \begin{pmatrix} 1 & j\frac{1}{B} \\ 0 & 1 \end{pmatrix} \begin{pmatrix} \cos\left(\frac{\psi}{2}\right) & \frac{j\sin\left(\frac{\psi}{2}\right)}{Y_0} \\ jY_0\sin\left(\frac{\psi}{2}\right) & \cos\left(\frac{\psi}{2}\right) \end{pmatrix} \tag{3.11}
$$

$$
\begin{pmatrix} A & B \\ C & D \end{pmatrix} = \begin{pmatrix} \cos\left(\frac{\psi}{2}\right) & \frac{j\sin\left(\frac{\psi}{2}\right)}{Y_0} \\ jY_0\sin\left(\frac{\psi}{2}\right) & \cos\left(\frac{\psi}{2}\right) \end{pmatrix} \begin{pmatrix} 1 & j\frac{1}{B} \\ 0 & 1 \end{pmatrix} \begin{pmatrix} \cos\left(\frac{\psi}{2}\right) & \frac{j\sin\left(\frac{\psi}{2}\right)}{Y_0} \\ jY_0\sin\left(\frac{\psi}{2}\right) & \cos\left(\frac{\psi}{2}\right) \end{pmatrix} \tag{3.12}
$$

We can have the following equations derived from ABCD matrices. Eq. 3.13 , Eq. 3.14 ,and Eq. 3.15 are the representation of K inverter,

$$
K = Z_0 \tan\left|\frac{\psi}{2}\right| \tag{3.13}
$$

$$
\psi = -\arctan\frac{2X}{Z_0} \tag{3.14}
$$

$$
\left|\frac{X}{Z_0}\right| = \frac{\frac{K}{Z_0}}{1 - \left(\frac{K}{Z_0}\right)^2} \tag{3.15}
$$

while Eq. 3.16 , Eq. 3.17 ,and Eq. 3.18 are the representation for J inverter.

$$
J = Y_0 \tan\left|\frac{\psi}{2}\right| \tag{3.16}
$$

$$
\psi = -\arctan\frac{2B}{Y_0} \tag{3.17}
$$

$$
\left|\frac{B}{Y_0}\right| = \frac{\frac{J}{Y_0}}{1 - \left(\frac{J}{Y_0}\right)^2} \tag{3.18}
$$

When we concentrate on the equations of K inverter, it is observed that X and $\psi/2$ will have opposite polarities. Because the characteristic impedances on the both side of X are equal so that above equations are quite simple. However, we will have some kind of constraints on filter design. To loose the constraints, the characteristic impedances on the both side of X are not necessary to be equal. The same analysis can be applied to J inverter. Next section will show the details of the asymmetric J and K inverter filters.

3.3 Asymmetric J and K Inverter Filters

We have introduced how to use equal impedance transmission lines with a lumped circuit shunt reactance or series suceptance in between to realize J and K inverter filters. Now, we want to use different impedance transmission lines instead. Naturally, the lengths of the transmission lines are varying with the impedances in the meanwhile. We can still write out the ABCD matrices and obtain relative equations by means of equalizing.
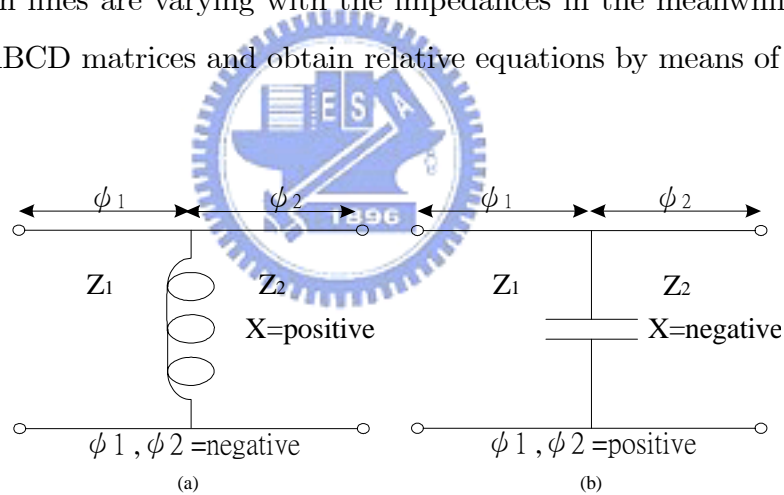

Figure 3-9: K inverters implementation with unequal impedance transmission lines besides the shunt reactance

41
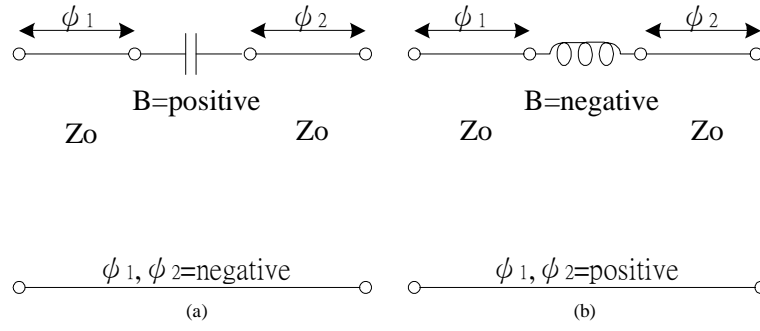
Figure 3-10: J inverters implementation with unequal impedance transmission lines besides the series susceptance

We can match Fig. 3-9 to K inverter and Fig. 3-10 to J inverter by equalizing the ABCD matrices. The ABCD matrix of K inverter and J inverter are the same as the previous section.

$$
\begin{pmatrix} A & B \\ C & D \end{pmatrix} = \begin{pmatrix} 0 & \pm jK \\ \pm j\frac{1}{K} & 0 \end{pmatrix}, \begin{cases} (+)when + 90° \\ (-)when - 90° \end{cases} \tag{3.19}
$$

$$
\begin{pmatrix} A & B \\ C & D \end{pmatrix} = \begin{pmatrix} 0 & \pm j\frac{1}{J} \\ \pm jJ & 0 \end{pmatrix}, \begin{cases} (+)when + 90° \\ (-)when - 90° \end{cases} \tag{3.20}
$$

The ABCD matrix of Fig. 3-9 and Fig. 3-8 are

$$
\begin{pmatrix} A & B \\ C & D \end{pmatrix} = \begin{pmatrix} \cos(\psi_1) & jZ_1\sin(\psi_1) \\ \frac{j\sin(\psi_1)}{Z_1} & \cos(\psi_1) \end{pmatrix} \begin{pmatrix} 1 & 0 \\ j\frac{1}{X} & 1 \end{pmatrix} \begin{pmatrix} \cos(\psi_2) & jZ_2\sin(\psi_2) \\ \frac{j\sin(\psi_2)}{Z_2} & \cos(\psi_2) \end{pmatrix} \tag{3.21}
$$

$$
\begin{pmatrix} A & B \\ C & D \end{pmatrix} = \begin{pmatrix} \cos(\psi_1) & \frac{j\sin(\psi_1)}{Y_1} \\ jY_1\sin(\psi_1) & \cos(\psi_1) \end{pmatrix} \begin{pmatrix} 1 & j\frac{1}{B} \\ 0 & 1 \end{pmatrix} \begin{pmatrix} \cos(\psi_2) & \frac{j\sin(\psi_2)}{Y_2} \\ jY_2\sin(\psi_2) & \cos(\psi_2) \end{pmatrix} \tag{3.22}
$$

42

We can have the following equations by equalizing ABCD matrices. Absolutely, the computation is more complicated than the case discussed in the last section. However, the degree of freedom increases. We can have various combinations of Z_1 and Z_2. Still, we can have the equations as follows from the matrices. Eq. 3.23 , Eq. 3.24 ,and Eq. 3.25 are the representation of K inverter,

$$\sin(\psi_1 - \psi_2) = \frac{K}{K^2 - Z_1 Z_2}(Z_1 - Z_2) \tag{3.23}$$

$$\sin(\psi_1 + \psi_2) = \frac{K}{K^2 + Z_1 Z_2}(Z_1 + Z_2) \tag{3.24}$$

$$X = -\frac{Z_1 Z_2}{Z_1 + Z_2}\tan(\psi_1 + \psi_2) \tag{3.25}$$

Simultaneously, Eq. 3.26 , Eq. 3.27 ,and Eq. 3.28 are the representation for J inverter.

$$\sin(\psi_1 - \psi_2) = \frac{J}{K^2 - Y_1 Y_2}(Y_1 - Y_2) \tag{3.26}$$

$$\sin(\psi_1 + \psi_2) = \frac{J}{J^2 + Y_1 Y_2}(Y_1 + Y_2) \tag{3.27}$$

$$B = -\frac{Y_1 Y_2}{Y_1 + Y_2}\tan(\psi_1 + \psi_2) \tag{3.28}$$

To this end, we can decide the characteristic impedance Z_1 and Z_2 to have relative ψ_1, ψ_2, and X of K inverter. Besides, we want to use an open-circuit stub to implement X. X is positive(inductive) for $l > \lambda_c/4$(quarter wavelength of the center frequency), and negative(conductive) for $l < \lambda_c/4$. Note that X will have opposite polarities of ψ_1 and ψ_2.We have known that the impedance of the open-circuit stub can be expressed as

$$Z_{in} = -jZ_0 \cot \beta l = jX \tag{3.29}$$

43

which means

$$Z_{open} = |X \tan \beta l| \qquad (3.30)$$

where Z_{open} and l are the characteristic impedance and the length of the open-circuit stub. However, the length of the open-circuit stub will decide the transmission zero frequency. The relation is shown as

$$\theta_{open} = \beta l = \frac{f_0}{f_z} \times 90° \qquad (3.31)$$

where f_0 is the center frequency and f_z is the transmission zero frequency. To conclude, we will obtain the value of ψ_1, ψ_2, and Z_{open} with given Z_1, Z_2, and λ_z (wavelength of the transmission zero frequency). Our design is focused on the K inverter, but the procedure of designing J inverter is almost the same.

Based on the considerations given above, a third-order filter, as shown in Fig. 3-11, can be designed. However, the coupled line stage with a small additional degree ψ_1 is not easy for tuning. As a result, we rearrange the network in Fig. 3-11 a little to the one in Fig. 3-12. We shorten the length of the coupled line to be a fixed degree θ_c, but keep the length of the first and last resonators to be $90°+\psi_1$.
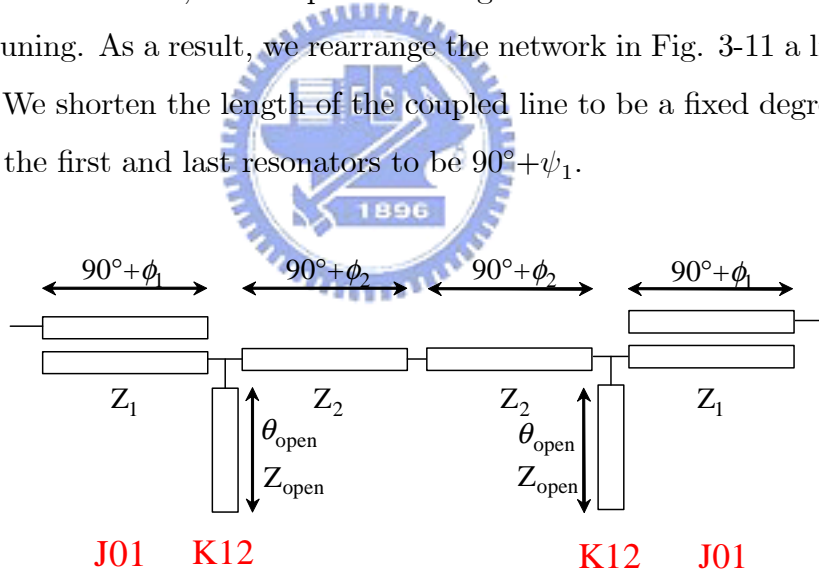

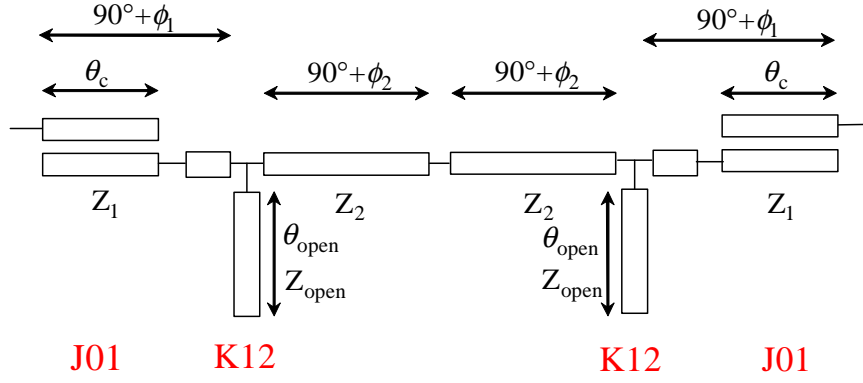Figure 3-11: Network of third order filter with proposed K inverter

Figure 3-12: Alternative network of third order filter with proposed K inverter

From Eq. 3.6 and Eq. 3.5 in section 3.1.2 , we can obtain that

$$J_{01} = \sqrt{\frac{b_{quarter}Y_0}{g_0 g_1} \times \Delta} \tag{3.32}$$

$$K_{12} = \sqrt{\frac{x_{quarter}x_{half}}{g_1 g_2} \times \Delta} \tag{3.33}$$

where $x_{quarter} = \frac{\pi Z_1}{4}$, $x_{quarter} = \frac{\pi Z_2}{2}$, and $b_{quarter} = \frac{\pi}{4Z_1}$. Also, we can compute Z_{oo} and Z_{oe} according to the Eq. 3.34 and Eq. 3.35.

$$Z_{oo_{01}} = Z_0 \left(1 - J_{01}Z_0 \csc(\theta_c) + (J_{01}Z_0)^2 \right) / \left(1 - (J_{01}Z_0 \cot(\theta_c))^2 \right) \tag{3.34}$$

$$Z_{oe_{01}} = Z_0 \left(1 + J_{01}Z_0 \csc(\theta_c) + (J_{01}Z_0)^2 \right) / \left(1 - (J_{01}Z_0 \cot(\theta_c))^2 \right) \tag{3.35}$$

In the end, we are well equipped for designing. The simulations and measurements of a K inverter filter with an upper stopband transmission zero and K-inverer filter with a lower stopband transmission zero will be presented in next two subsections.

3.3.1 K Inverter Filter with Upper-Stopband Transmission Zero

Firstly, we have to decide the characteristic impedances of the microstrip lines on the either side of the reactance implemented by an open-circuit stub. Then, the value of J_{01} and K_{12} can be obtained on the basis of the Eq. 3.32 and 3.33 in the previous section. We set Z_1 to be 50Ω, which matches the port impedance of the system. We can have relative ψ_1, ψ_2, and X from Eq. 3.23 , Eq. 3.24 ,and Eq. 3.25 by arranging Z_2. Next, we choose the frequency of the transmission zero f_z to be located in the upper stop-band. θ_{open} and Z_{open} will be settle down at the same time. The list of the Z_{open}, ψ_1,and ψ_2 varying with the Z_2 are shown as below. Fig. 3-14 also depicts the relations between Z_2 and Z_{open}. The open-circuit stub is regarded as a capacitor when $\theta_{open} < 90°$. It means the reactance is negative, which results in ψ_1 and ψ_2 to be positive degree. The list also shows the good agreement with our supposition. And we will expect a transmission zero occurring at higher stop-band.

f_z=2.464GHz, θ_{open}=83°			
$Z_2(\Omega)$	$Z_{open}(\Omega)$	$\phi_1(°)$	$\phi_2(°)$
20	19.37	2.56	6.45
35	25.57	3.39	4.86
50	30.56	4.06	4.06
65	34.95	4.65	3.56
80	38.68	5.15	3.21

Figure 3-13: Z_{open}, ψ_1,and ψ_2 varying with Z_2 at f_z= 2.464GHz
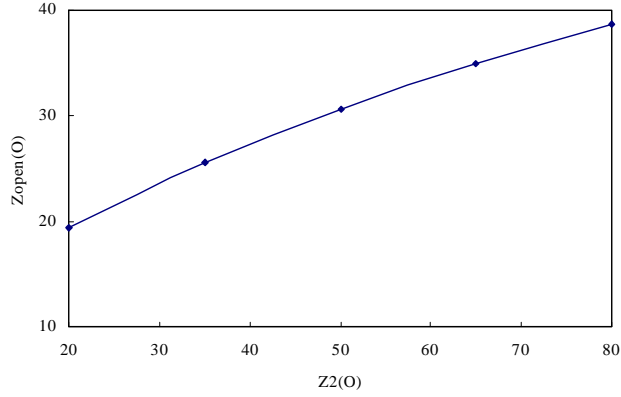
Figure 3-14: Variation of Z_{open} with Z_2 at f_z= 2.464GHz

Now, we have the Z_1, Z_2, Z_{open}, θ_{open}, ψ_1, and ψ_2, the rest are the $Z_{oo_{01}}$, $Z_{oe_{01}}$ which can be decided according to Eq. 3.34 and Eq. 3.35. Thus, all the parameters are ascertained. Next step is to fabricate a filter to validate our design method. We aim at the filter with bandwidth Δ=5% and passband ripple=0.01dB. Fig. 3-15 and Fig. 3-16 are the simulated scheme and frequency response in AWR. Further, simulated scheme and frequency response in Sonnet are illustrated in Fig. 3-17 and Fig. 3-18.
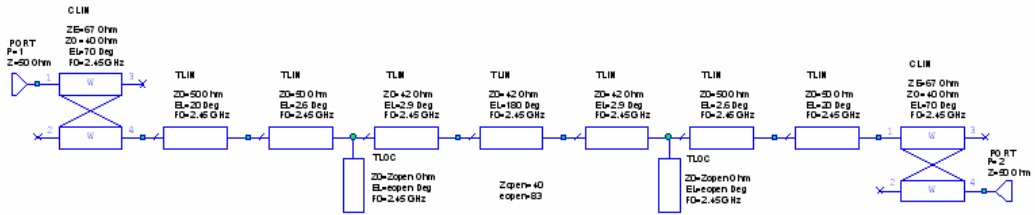

Figure 3-15: Simulated schematic circuit of third-order K inverter filter with an upper-stopband transmission zero in AWR
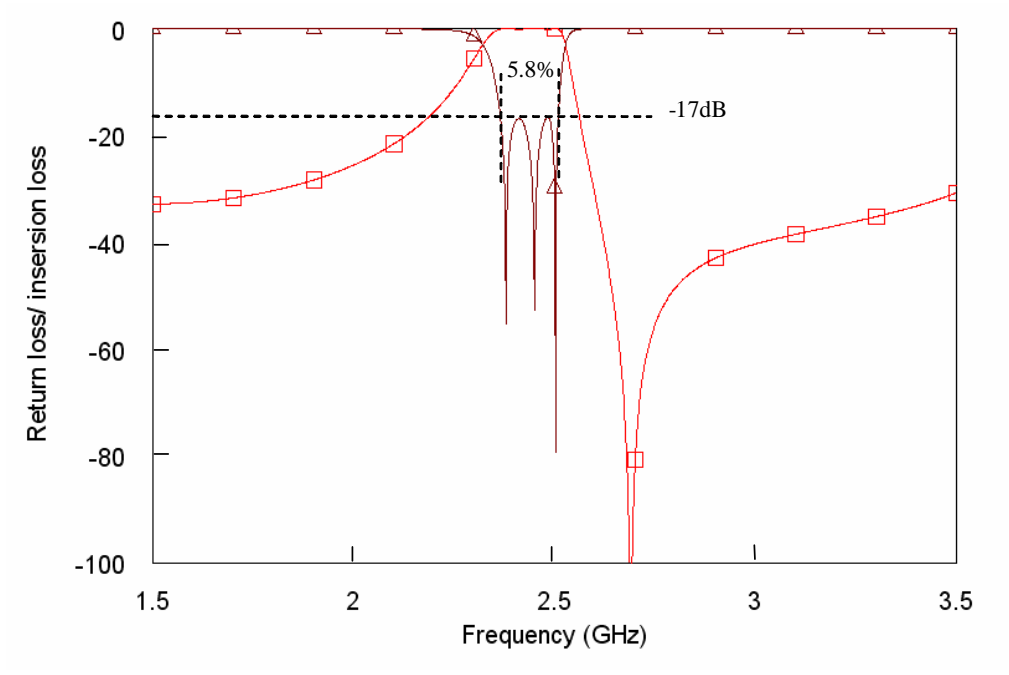
47

Figure 3-16: Simulated frequency response of third-order K inverter filter with an upper-stopband transmission zero in AWR
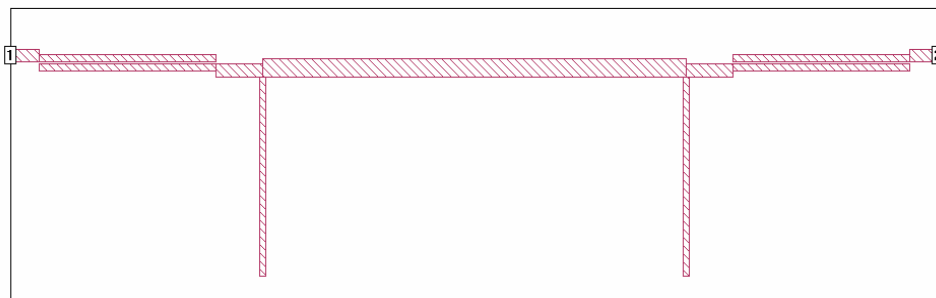

Figure 3-17: Simulated physical layout of third-order K inverter filter with an upper-stopband transmission zero in Sonnet
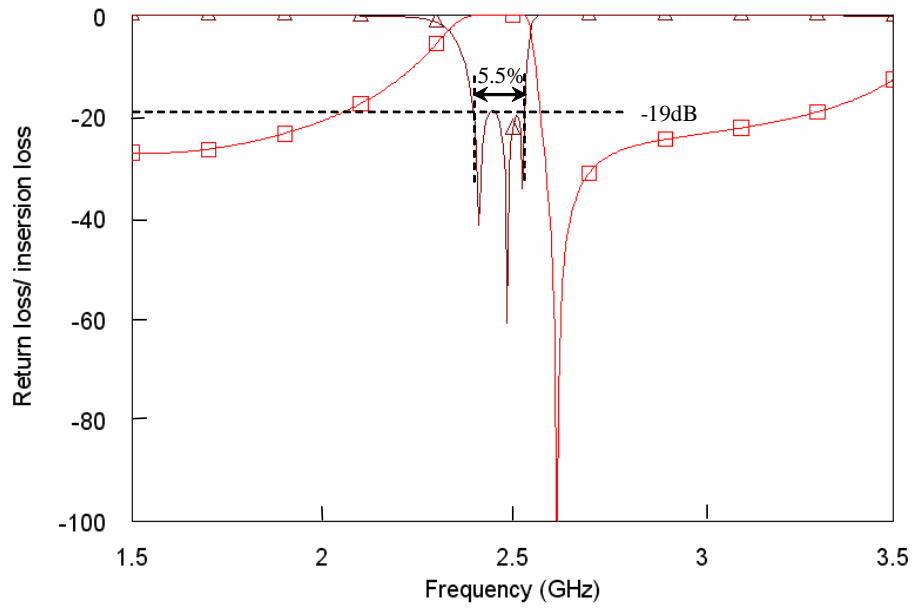
Figure 3-18: Simulated frequency response of third-order K inverter filter with an upper-stopband transmission zero in Sonnet

Finally, the photograph of filter with asymmetric K inverter is shown in Fig. 3-19 and the experimental result is depicted in Fig. 3-20. The measured data shows that the in-band return insertion loss is 1.7dB and the return loss is 16.5dB. Comparing to the simulation, the response has slightly extended bandwidth $\Delta=6.2\%$. We validate the method of designing filter with K inverter.

Figure 3-19: Photograph of third-order K inverter filter with an upper-stopband transmission zero

Figure 3-20: Measured frequency response of third-order K inverter filter with an upper-stopband transmission zero

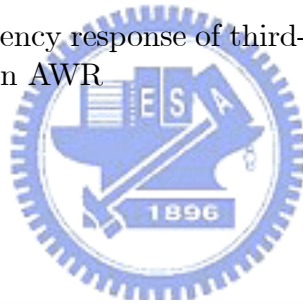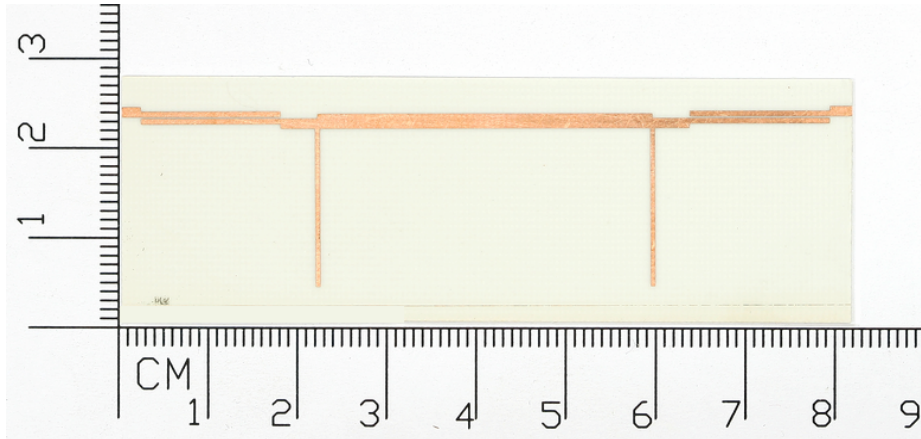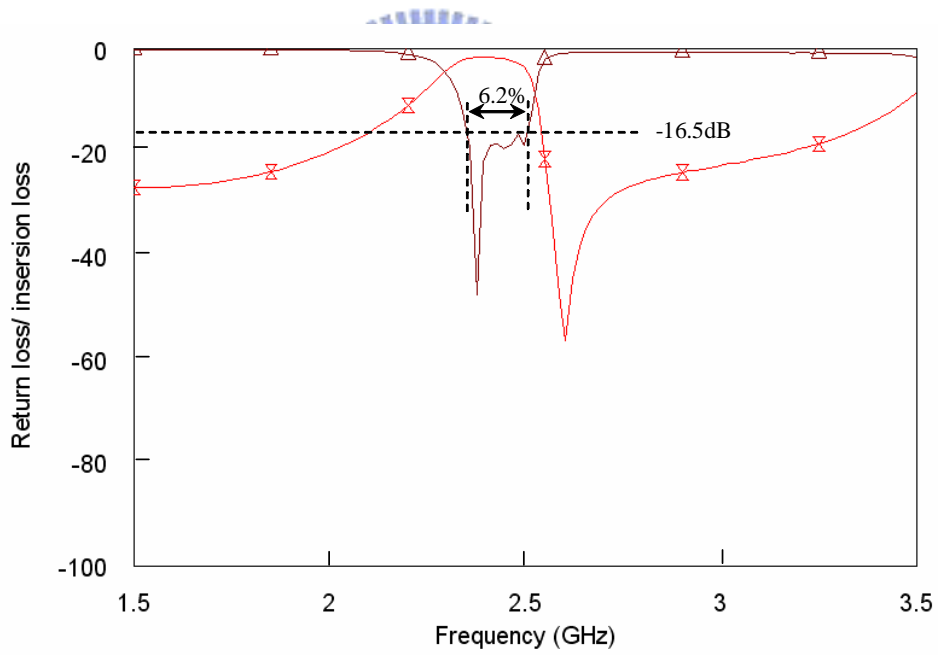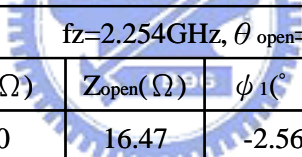### 3.3.2 K Inverter Filter with Lower-Stopband Transmission Zero

Tracing the same procedure of designing K inverter filter with lower stopband transmission zero, we have to decide the characteristic impedances of the microstrip lines on the either side of the reactance implemented by an open-circuit stub. Then, the value of J_{01} and K_{12} can be obtained on the basis of the Eq. 3.32 and 3.33 . We set Z_1 to be 50Ω, which matches the port impedance. We can have relative ψ_1, ψ_2, and X from Eq. 3.23 , Eq. 3.24 ,and Eq. 3.25 by arranging Z_2. Next, we choose the frequency of the transmission zero f_z to be located in the lower stop-band. θ_{open} and Z_{open} will be settle down in the meanwhile. The list of the Z_{open}, ψ_1,and ψ_2 varying with the Z_2 are shown as below. Fig. 3-22 also depicts the relations between Z_2 and Z_{open}. The open-circuit stub is regarded as a inductor when $\theta_{open} > 90°$. It means the reactance is positive, which results in ψ_1 and ψ_2 to be negative degree. The list also shows the good agreement with our supposition. And we will expect a transmission zero occurring in the lower stop-band.

fz=2.254GHz, θ open=98°			
$Z_2(\Omega)$	$Z_{open}(\Omega)$	$\phi_1(°)$	$\phi_2(°)$
20	16.47	-2.56	-6.45
35	21.75	-3.39	-4.86
50	25.99	-4.06	-4.06
65	29.64	-4.65	-3.56
80	32.89	-5.15	-3.21

Figure 3-21: Z_{open}, ψ_1,and ψ_2 varying with Z_2 at f$_z$= 2.254GHz
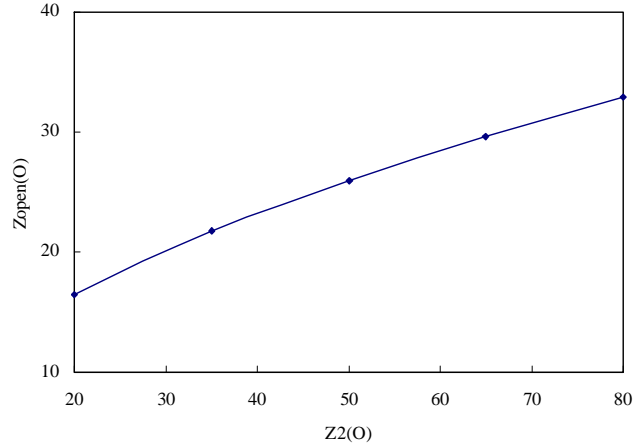
Figure 3-22: Variation of Z_{open} with Z_2 at f_z= 2.254GHz

Now, we have the Z_1, Z_2, Z_{open}, θ_{open}, ψ_1,and ψ_2, the rest are the $Z_{oo_{01}}$, $Z_{oe_{01}}$ which can decided according to Eq. 3.34 and Eq. 3.35. Thus, all the parameters are ascertained. Next step is to fabricate a filter to validate our design method. We target at the filter with bandwidth Δ=5% and passband ripple=0.01dB. Fig. 3-23 and Fig. 3-24 are the simulated schematic circuit and frequency response in AWR.

Figure 3-23: Simulated schematic circuit of third-order K inverter filter with a lower-stopband transmission zero in AWR

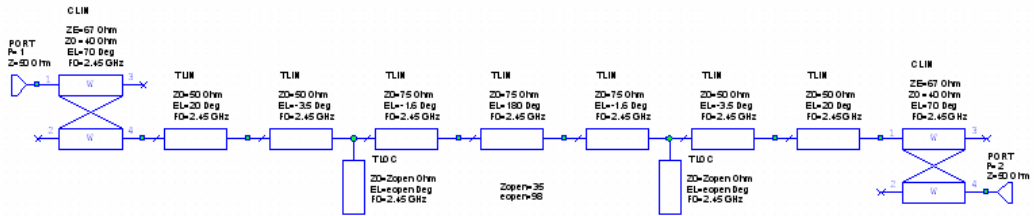Figure 3-24: Simulated frequency response of third-order K inverter filter with a lower-stopband transmission zero in AWR

Although Z_{open} raise along with Z_2, we find that Z_{open} is still too small. This will make the linewidth of the open-circuit stub too wide to implement. We need to do some adjustment about the layout. We suggest that a single open-circuit stub with the characteristic impedance Z_{open} can be transformed to two parallel open-circuit stubs with characteristic impedance $2Z_{open}$. In addition, we add the transitions to where the open-circuit stubs taper in, and we revise the length of the stubs. The layout after changes is exhibited as Fig. 3-25, which is the simulated scheme in Sonnet. The result of the simulation in Sonnet is presented in Fig. 3-26 as well.

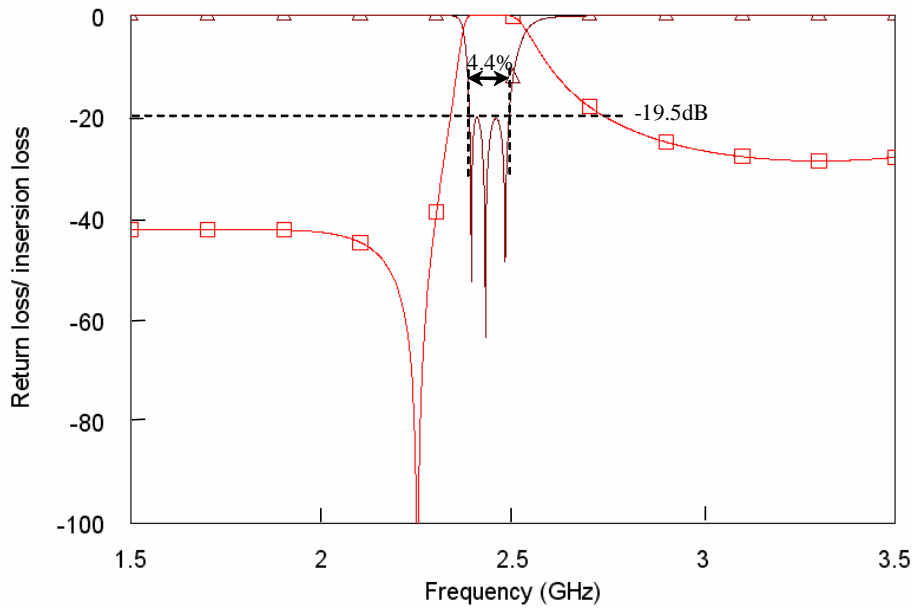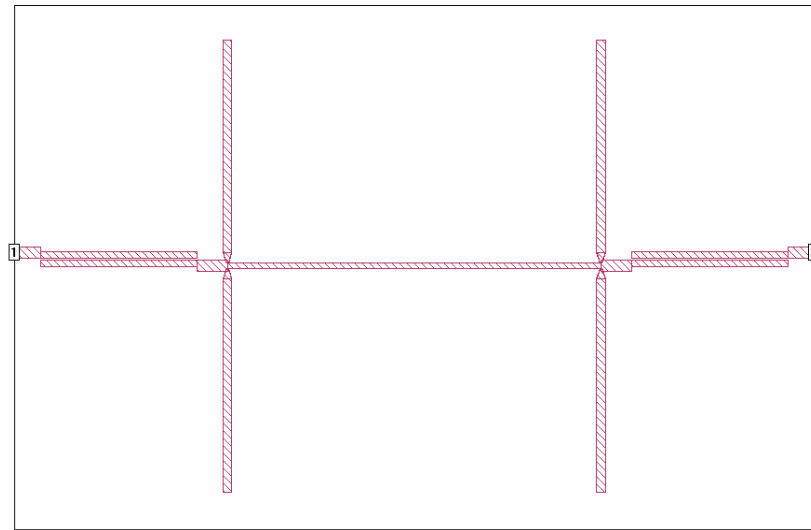Figure 3-25: Simulated physical layout of third-order K inverter filter with a lower-stopband transmission zero in Sonnet
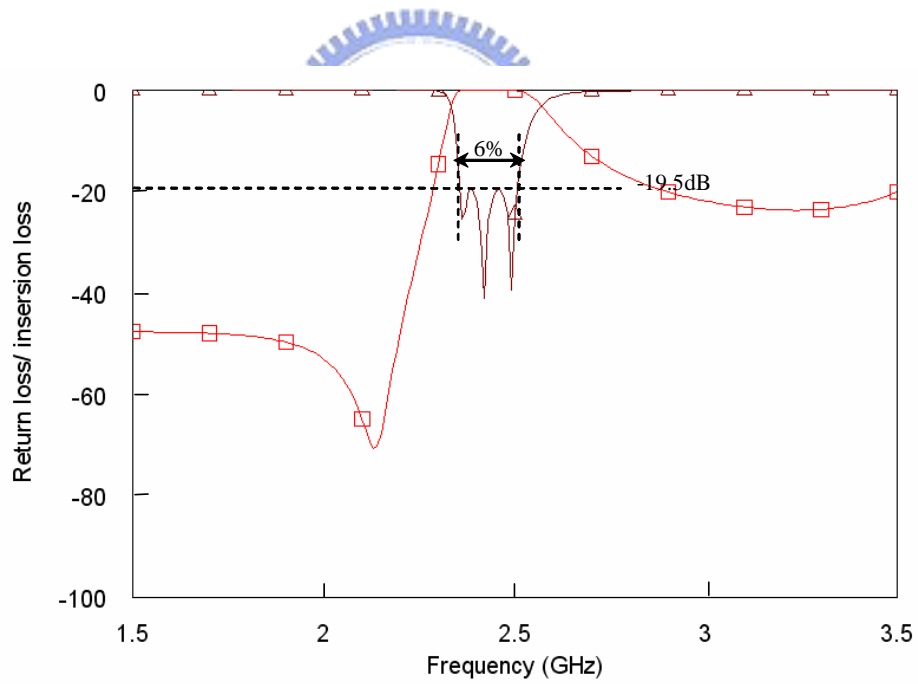
Figure 3-26: Simulated frequency response of third-order K inverter filter with a lower-stopband transmission zero in Sonnet

At last the photograph of the filter with asymmetric K inverter and lower stopband transmision zero is displayed in Fig. 3-27. And the experimental result is depicted in Fig. 3-28. The measured data shows that the in-band return insertion loss is 1.7dB and the return loss is 23dB. Comparing to the simulation, the response has slightly shrunk bandwidth $\Delta=5.5\%$. Hence it can be concluded that the designing method in this chapter can be applied on both the K inverter filter with an upper stopband transmission zero and the K inverter filter with a lower stopband transmission zero.

Figure 3-27: Photograph of third-order K inverter filter with a lower-stopband transmission zero
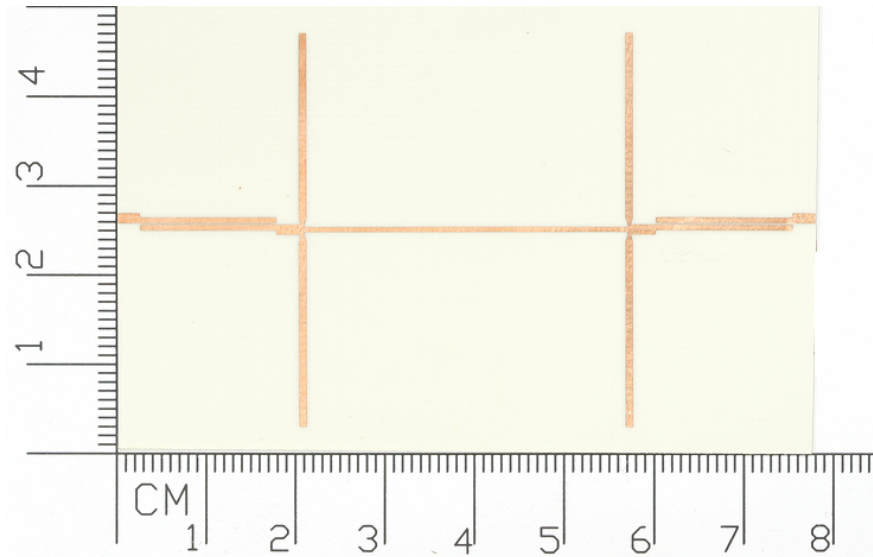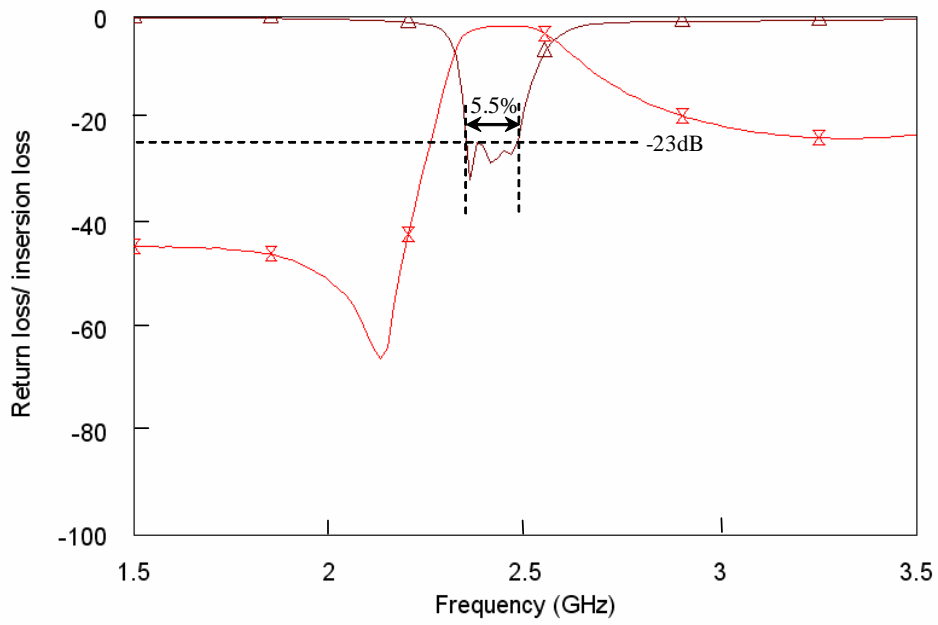
Figure 3-28: Measured frequency response of third-order K inverter filter with a lower-stopband transmission zero

Chapter 4

Conclusion

In Chapter 2, we submit a novel structure for multiple-mode resonator filters. Both of the tri-mode filter with an upper-stopband tranmission zero and the tri-mode filter with a lower-stopband tranmission zero have been synthesized and implemented by multi-mode resonator method. The resonant frequencies of the proposed multiple-mode have been allocate to match the transmission poles of the of a Chebyshev pass-band. It has been validated that a configurable transmission zero can be decided by an open-circuit stub with a small short-circuit stub or a capacitor in parallel. The simulations and measurements of the tri-mode filters with center frequency 2.45GHz and fractional bandwidth Δ=20% are presented. The measured frequency responses match well with the simulated ones. Despite the advantages such as compact size, systematic design procedure, and high selectivity, the proposed tri-mode resonator filters can push the transmission zero frequency to three times higher than the center frequency. Furthermore, the triple-mode filter with a upper-stopband tranmission zero has one more desirable property- excellent rejection ability for low frequency signal.

In Chapter 3, a completely different method of synthesizing filters has been introduced. We fabricated the filters with K inverter which are formed by two different impedances and lengths microstrip lines with centered open-circuit stub. All the required parameters can be determined by equalizing the ABCD matrices. If the stub is shorter

than the quarter wavelength of center frequency, it can be seen as a negative reactance resulting an upper stopband transmission zero. On the other hand, the stub longer than the quarter wavelength of center frequency will lead to a lower-stopband transmission zero. The experiments of making the third order filters with center frequency 2.45GHz and fractional bandwidth Δ=5% indicate the method is more flexible than the conventional design.

Although both methods of filter design can achieve third order filter with tunable transmission zero, the former has more elegant properties such as smaller size, wider pass-band range, wider upper stop-band range, and higher out-of-band rejection ratio. Accordingly, the multimode resonator filters are more attractive to commercial applications.

Bibliography

[1] David M. Pozar, *Microwave Engineering,* 3rd ed. New York:Wiley, 2005.

[2] L. Zhu, H. Bu, and K. Wu, "Aperture compensation technique for innovative design of ultra-broadband microstrip bandpass filter," in *IEEE MTT-S Int. Dig.*, pp.315-318, Jun. 2000.

[3] W. Menzel, L. Zhu, and K. Wu, "On the design of novel compact broad-band planar filters," in *IEEE Tran. Microw. Theory Tech*, vol. 51, no. 2, pp.364-370, Feb. 2003.

[4] L. Zhu, S. Sun, and W. Menzel, "Ultra-wideband (UWB) bandpass filters using multiple-mode resonator," in *IEEE Microw. Wireless Compon. Lett.*, vol. 15, no. 11, pp.796-798, Nov. 2005.

[5] L. Zhu and H.Wang, "Ultra-wideband (UWB) bandpass filter on aperture-backed microstrip line," in *Electron. Lett.*, vol. 41, no. 18, pp.1015-1016, Sep. 2005.

[6] L. Zhu, H.Wang, and W. Menzel, "Ultra-wideband (UWB) bandpass filters with hybrid microstrip/CPW structure," in *IEEE Microw. Wireless Compon. Lett.*, vol. 15, no. 12, pp.844-846, Dec. 2005.

[7] Y.-C. Chiou and J.-T. Kuo, "Broadband quasi-Chebyshev bandpass filters with multimode stepped-impedance resonators (SIRs)," *IEEE Tran. Microw. Theory Tech*, vol. 54, no. 8, pp.3352-3358, Aug. 2006.

[8] R. Li and L. Zhu, "Compact UWB Bandpass Filter Using Stub-Loaded Multiple-Mode Resonator," in *IEEE Microw. Wireless Compon. Lett.*, vol. 17,no. 1, pp.421-423 Jan. 2007.

[9] S.- W. Wong and L. Zhu, "EBG-Embedded Multiple-Mode Resonator for UWB Bandpass Filter With Improved Upper-Stopband Performance," in *IEEE Microw. Wireless Compon. Lett.*, vol. 17, no. 6, pp.40-42, Jun. 2007.

[10] M.-H. Ren, D. Chen, C.-H. Cheng, "A novel wideband bandpass filter using a cross multiple-mode resonator," in *IEEE Microw. Wireless Compon. Lett.*, vol. 18, no. 1, pp.13-15, Jan. 2008.

[11] S.- W. Wong and L. Zhu, "Implementation of Compact UWB Bandpass Filter With a Notch-Band," in *IEEE Microw. Wireless Compon. Lett.*, vol. 18, no. 1, pp.10-12, Jan. 2008.

[12] G. L. Matthaei, L. Young, and E. M. T. Jones, *Microwave Filters, Impedance-Matching Network, and Coupling Structures.* Norwood, MA: Artech House, 1980.

[13] J.-R. Lee, J.-H. Cho, and S.-W. Yun, "New Compact Bandpass Filter Using Microstrip $\lambda/4$ Resonators with Open Stub Inverter," in *IEEE Microw. and Guided Wave Lett.*, vol. 10, no. 12, pp.526-527, Dec. 2000.